crystals

MDPI

Review

Pressure-Induced Phase Transitions in Sesquioxides

Francisco Javier Manjón [1,*], Juan Angel Sans [1], Jordi Ibáñez [2] and André Luis de Jesús Pereira [3]

1 Instituto de Diseño para la Fabricación y Producción Automatizada, MALTA-Consolider Team, Universitat Politècnica de València, 46022 Valencia, Spain; juasant2@upv.es
2 Institute of Earth Sciences Jaume Almera, MALTA-Consolider Team, Consell Superior d'Investigacions Científiques (CSIC), 08028 Barcelona, Catalonia, Spain; jibanez@ictja.csic.es
3 Grupo de Pesquisa de Materiais Fotonicos e Energia Renovável—MaFER, Universidade Federal da Grande Dourados, Dourados 79825-970, MS, Brazil; andreljpereira@gmail.com
* Correspondence: fjmanjon@fis.upv.es; Tel.: +34-699-133-078

Received: 12 November 2019; Accepted: 26 November 2019; Published: 28 November 2019

Abstract: Pressure is an important thermodynamic parameter, allowing the increase of matter density by reducing interatomic distances that result in a change of interatomic interactions. In this context, the long range in which pressure can be changed (over six orders of magnitude with respect to room pressure) may induce structural changes at a much larger extent than those found by changing temperature or chemical composition. In this article, we review the pressure-induced phase transitions of most sesquioxides, i.e., A_2O_3 compounds. Sesquioxides constitute a big subfamily of ABO_3 compounds, due to their large diversity of chemical compositions. They are very important for Earth and Materials Sciences, thanks to their presence in our planet's crust and mantle, and their wide variety of technological applications. Recent discoveries, hot spots, controversial questions, and future directions of research are highlighted.

Keywords: sesquioxides; high pressure; phase transitions

1. Introduction

The family of sesquioxides (SOs), i.e., compounds with A_2O_3 stoichiometry, is very important from an applied point of view, since SOs play a vital role in the processing of ceramics as additives, grain growth inhibitors and phase stabilizers. They also have potential applications in nuclear engineering and as hosts for optical materials for rare-earth (RE) phosphors. Besides, SOs with corundum-like structure, like corundum (α-Al_2O_3), hematite (α-Fe_2O_3) and eskolaite (α-Cr_2O_3), are relevant to Earth and planetology Sciences, because they are minerals present in the Earth's crust or in meteorites. Therefore, knowledge and understanding of phase transitions (PTs) occurring at high pressure (HP) in SOs is very important for Physics, Chemistry and Earth and Materials Sciences.

SOs are mainly formed by materials featuring an A cation of valence 3+, so that the two A cations compensate the total negative valence (6−) of three O atoms acting with valence 2−. Among the cations featuring 3+ valence, we find all group-13 and group-15 elements, some transition metal (TM) elements and all RE elements. Additionally, we can also find SOs where cations show an average 3+ valence. In this context, SOs with cations showing both 2+ and 4+ valences (both valences present in the A_2O_3 compound), are named mixed-valence (MV) SOs. The different compositions of these compounds provide a very rich environment ranging from molecular or zero-dimensional (0D), one-dimensional (1D) and two-dimensional (2D) solids to the conventional (bulk) three-dimensional (3D) solids; all of them showing radically different properties and behaviors under compression.

After more than 50 years of exploration of pressure-induced PTs in SOs, we present in this work a review of the PTs of SOs at HP, including those occurring at high temperatures (HTs), at low

temperatures like room temperature (RT), and even at room pressure (RP). We have structured the present paper in five main sections that are devoted to RE-SOs, group-13-SOs, group-15-SOs, TM-SOs, and MV-SOs.

Finally, before attempting to present our results, we must comment that several reviews of the PTs in SOs at HP have been already published. We can cite the review on oxides of Liu and Basset in 1986 [1], of Adachi and Imanaka in 1998 [2], of Smyth et al. in 2000 [3], of Zinkevich in 2007 [4] and of Manjón and Errandonea in 2009 [5]. The present review goes beyond previous studies of SOs by expanding the number of families studied, by discussing the most recent results published in the last decade, and by suggesting pressure-based studies still to be performed.

2. High-Pressure Phase Transitions in Sesquioxides

2.1. Rare-Earth Sesquioxides

RE-SOs are highly interesting and versatile for different types of applications, since the atomic radius can be finely tuned along the lanthanide family, thus enabling a wide range of technological applications, including light emitters (lasers and improved phosphors), catalysts, and high-dielectric constant (high-k) gates.

RE-SOs, and in particular lanthanide SOs (Ln_2O_3; Ln = La to Lu, including Y and Sc), usually crystallize at room conditions in either the A-, B-, or C-type structures, depending on the RE atomic size. Large cations from La to Nd usually crystallize in the trigonal A-type structure (s.g. $P\bar{3}m1$), medium-size cations from Sm to Gd tend to show a monoclinic B-type structure (s.g. $C2/m$), and small cations from Tb to Lu, including Sc and Y, tend to adopt a cubic C-type structure (s.g. $Ia\bar{3}$). At HTs, two additional phases, hexagonal H (s.g. $P6_3/mmc$) and cubic X (s.g. $Im\bar{3}m$) structures, have also been found in Ln_2O_3 [6]. Zinkevich has reviewed temperature-induced PTs in RE-SOs and found that a C→B→A sequence of PTs usually occurs upon an increase in temperature [4]. Since the density and cation coordination of the A-, B- and C-type structures increase in the sequence C-B-A, C→B, B→A, and even direct C→A transitions are expected on increasing pressure (upstroke), while inverse PTs are expected on decreasing pressure (downstroke) [7,8]. Curiously, it has been found that the cationic distances in the three structures of the RE-SOs at room conditions are similar to those in the bcc, fcc and hcp structures of the RE metals, thus suggesting that a relationship must exist between them [9,10].

The effect of HP on Ln_2O_3 has been extensively studied by many research groups, mainly by X-ray diffraction (XRD), Raman scattering (RS) and photoluminescence measurements. The HP behavior of C-type compounds has been studied in Lu_2O_3 [11–14], Yb_2O_3 [15–18], Tm_2O_3 [19,20], Er_2O_3 [11,21,22], Ho_2O_3 [23–26], Dy_2O_3 [27,28], Gd_2O_3 [11,29–36], Eu_2O_3 [11,37–43], Sm_2O_3 [11,32,44,45], Sc_2O_3 [46–48], Y_2O_3 [11,32,49–60], and recently on Tb_2O_3 [61]. Examples of pressure-driven C→B, B→A, direct C→A, and even C→A+B transitions have been shown to occur in a number of RE-SOs. As example, Lu_2O_3 was found to show either a C→B PT around 12 GPa without B→A PT up to 47 GPa [12,13], or a C→A+B PT above 25 GPa, with a recovery of a single B phase on downstroke from 47 GPa [14]. Similarly, Yb_2O_3 was found to exhibit a C→B PT above 13 GPa, and no further PT was found up to 20 GPa [15], but an A phase was found above 19.6 GPa that transforms into the B phase below 12 GPa [16]. The A phase in coexistence with the B phase was confirmed by RS measurements up to 45 GPa [17]. The C→B→A sequence of PTs was also found in Y_2O_3, the most studied RE-SO at HP, around 12 and 19 GPa [49], and has been confirmed in many studies [60]. In this context, it must be stressed that the pressure-induced PT sequence in Y_2O_3 has been shown to be affected by the nature of the sample, since different sequences of PTs have been observed in nanocrystals [33]. It must be stressed that direct C→A PT, with A→B PT on downstroke from 44 GPa, has been observed in Sm_2O_3 [44]. This sequence of PTs has also been observed in Gd_2O_3 [31]. Other PTs in RE-SOs have been found at HP and HT. In particular, an orthorhombic Gd_2S_3-type structure (s.g. *Pnma*) has been found in C-type Y_2O_3 above 8 GPa [57].

The HP behavior of B-type compounds has been also studied in Y_2O_3 [62], Eu_2O_3 [63], and Sm_2O_3 [64,65]. A reversible pressure-induced B→A PT has been observed in all B-type compounds. Additionally, the Gd_2S_3-type structure has been found in B-type Sc_2O_3 above 19 GPa upon laser heating [47]. Table 1 summarizes the experimental PT pressures observed in C- and B-type RE-SOs.

Table 1. Experimental data of the phase transition pressures (in GPa) for Ln_2O_3 and related sesquioxides having a C- or B-type phase at room conditions. The measurement technique (Tech.) and the pressure-transmitting medium (PTM) are also provided. Comp. stands for compound, MEW stands for the 16:3:1 mixture of methanol:ethanol:water and Polyethy. stands for polyethylene glycol.

Comp.	$P_{C\rightarrow A}$	$P_{C\rightarrow B}$	$P_{B\rightarrow A}$	Tech.	PTM	Reference
Sc_2O_3		36		XRD	MEW	[46]
		25–28		XRD	Neon	[48]
Lu_2O_3	14			XRD	N_2	[11]
		12.7–18.2		XRD	Silicon Oil	[12]
		17.0–21.4		XRD	ME	[13]
Yb_2O_3		13		XRD	Silicon Oil	[15]
	30–47	14	11.9	XRD	MEW	[14,16]
	17.0			XRD	N_2	[11]
	20.6			RS	ME	[18]
Tm_2O_3		7		XRD	MEW	[19]
		12		XRD	MEW	[20]
Er_2O_3		9.9–16.3		XRD	Silicon Oil	[66]
	14			XRD	N_2	[11]
	17.8–20.0	13.6	17.8–23.5	XRD	He	[22]
		6.6–12.7	22.5–42.0	XRD	Silicon Oil	
Y_2O_3	13.0			XRD	N_2	[11]
	15.0–25.6	15.0–25.6	14.3–17.5	XRD	MEW	[57]
			23.5–44.0	XRD	Neon	[62]
		13	24.5	XRD	No PTM	[54]
Ho_2O_3		8.9–16.3	14.8–26.4	XRD	Silicon Oil	[24]
		9.5		XRD	MEW	[19]
		9.5–16.0		XRD	MEW	[23]
		8.8		XRD	MEW	[20]
Dy_2O_3		7.7–18.8	10.9–26.6	XRD	Silicon Oil	[28]
Tb_2O_3		7	12	XRD	MEW	[61]
Gd_2O_3	7.0–15.0		6.8	XRD	MEW	[31]
	8.9–14.8	2.5	8.9	XRD	Ar	[33]
	7.0			XRD	N_2, Ar, He	[11]
	8.6–12.5		5.1	XRD	Silicon Oil	[34]
	12.0			XRD	MEW	[19]
Eu_2O_3			4.7	XRD	Silicon Oil	[63]
	5.0–13.1			XRD	Silicon Oil	[40]
	6.0			XRD	N_2	[11]
	5.7–12.9			XRD	MEW	[41,42]
Sm_2O_3			3.2–3.9	XRD	Polyethy.	[64]
	7.5–12.5		4.7	XRD	Silicon Oil	[44]
	4.0			XRD	N_2, Ar	[11]
	4.2		2.5	XRD	Silicon Oil	[45]

The HP behavior of A-type compounds has been studied in Nd_2O_3 [67,68], Ce_2O_3 [69], and La_2O_3 [11]. A-type Nd_2O_3 has been observed to suffer a reversible PT above 27 GPa towards a monoclinic s.g. *P2/m* phase [67]. However, other work has suggested a 1st-order isostructural PT

above 10 GPa [68]. This behavior is in contrast with that of Ce_2O_3, which seems to be stable in the A-type phase up to 70 GPa. Curiously, A-type Ce_2O_3 shows anomalies in the compressibility of the lattice parameters around 20 GPa, which could be related to an isostructural PT similar to that of Nd_2O_3. Finally, A-type La_2O_3 seems not to be stable above 4 GPa, following a PT to a hexagonal superlattice and eventually to a distorted monoclinic structure with a group–subgroup relationship with the hexagonal one [11].

It must be mentioned that RE-SOs and their pressure-induced PTs have also been investigated theoretically, and the simulations of the bandgap, volume, bulk modulus and its pressure derivative for the C, B and A phases, as well as their PT pressures, have been reported and found in rather good agreement with experiment [70–83]. Theoretical studies have found that the C→A and C→B PTs result in a decrease in the unit cell volume per formula unit at the transition pressure of the order of 10% ± 2%, in good agreement with experiments [81]. On the other hand, the B→A PT results in a decrease in the unit cell volume per formula unit at the transition pressure of the order of less than 2%, in good agreement with experiments [76]. Figures 1–3 show a comparison of experimental data (from Table 1) and theoretical data for the C→A, C→B and B→A PT pressures in bulk RE-SOs as a function of the atomic number of the lanthanide, Z_{Ln}, and of the ionic radius of the RE cation. In general, a good agreement between theoretical and experimental data can be found for all PTs. As regards the C→A PT, the pressure of the transition increases along the lanthanide series with the increase in atomic number, i.e., with the decrease in the ionic radius. It must be noted that no work has reported the C→A PT for Sc_2O_3, and that the reported C→A PT in materials with a small ionic radius, like Lu_2O_3 and Yb_2O_3, are doubtful. Regarding the C→B PT, the pressure of the transition also increases along the lanthanide series with the increase in atomic number or the decrease in the ionic radius. Unfortunately, no theoretical data exist for the C→B PT along the whole RE-SOs series; consequently, theoretical data for the C→A PTs are plotted for comparison with experimental data of the C→B PTs. It must be noted that the C→B PT is not observed in Sm_2O_3 and Eu_2O_3, since these two SOs undergo a direct C→A PT. Finally, as regards the B→A PT, the pressure of the transition once again increases along the lanthanide series with the increase in atomic number or the decrease in the ionic radius. As observed, no experimental data for the B→A PT has been reported in Sc_2O_3, Lu_2O_3 and Tm_2O_3. This will require new experiments up to 40 GPa in Lu_2O_3 and Tm_2O_3 and above 80 GPa in Sc_2O_3.

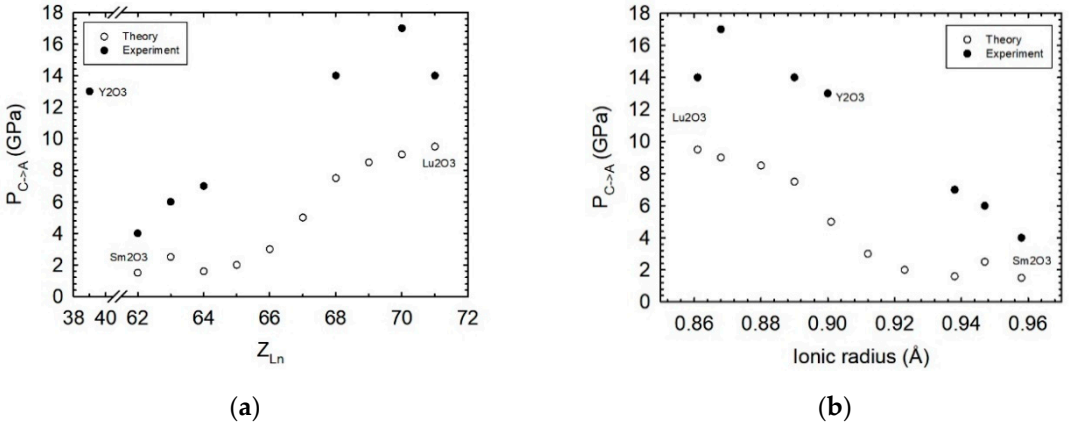

Figure 1. Experimental (solid symbols) and theoretical (empty symbols) data for the C→A phase transition pressures in Ln_2O_3 and related sesquioxides as a function of (**a**) the atomic number, Z_{Ln}, and (**b**) the ionic radius. Experimental data are from Table 1, while theoretical data are from reference [81]. Ionic radii of Shannon for cation 6-fold coordination were considered.

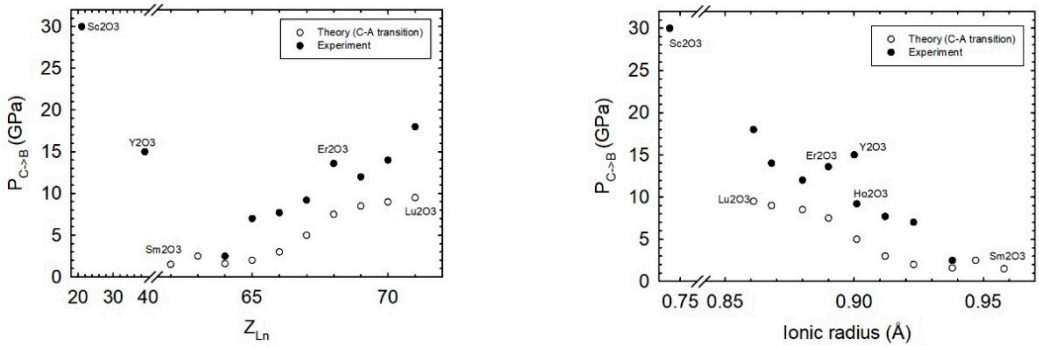

Figure 2. Experimental (solid symbols) and theoretical (empty symbols) data for the C→B phase transition pressures in Ln_2O_3 and related sesquioxides as a function of (**a**) the atomic number, Z_{Ln}, and (**b**) the ionic radius. Experimental data are from Table 1, while theoretical data correspond to those of the C→A phase transition in reference [81], since no theoretical data for the C→B phase transition are known to our knowledge. Ionic radii of Shannon for cation 6-fold coordination were considered.

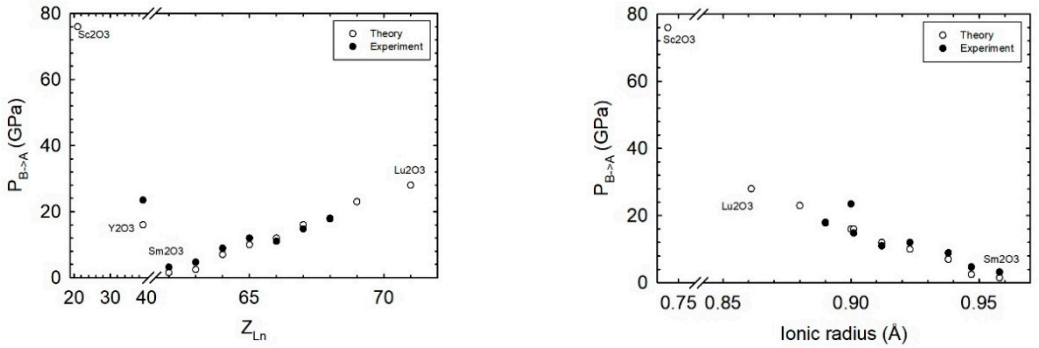

Figure 3. Experimental (solid symbols) and theoretical (empty symbols) data for the B→A phase transition pressures for Ln_2O_3 and related sesquioxides as a function of (**a**) the atomic number, Z_{Ln}, and (**b**) the ionic radius. Experimental data are from Table 1, while theoretical data are from reference [76]. Ionic radii of Shannon for cation 6-fold coordination were considered.

In summary, there are many HP studies in cubic C-type RE-SOs that allow us to conclude that this structure undergoes a pressure-induced irreversible 1st-order PT either to a hexagonal A-type structure or to an intermediate monoclinic B-type structure. It is also observed that the A-type structure of RE-SOs usually reverts to the B-type structure on decreasing pressure, but the B-type structure remains metastable at room conditions and does not revert to the C-type structure unless it is conveniently heated. The irreversibility of the C→A and C→B PTs means that there is a considerable kinetic energy barrier between the C-type and the A- and B-type structures, due to the reconstructive nature of these PTs. On the other hand, the reversibility of the B→A PT is consequence of the weak 1st-order nature of this PT, as expected, because A- and B-type structures obey a group-subgroup relationship. In this context, HP studies of B-type RE-SOs show a pressure-induced reversible weak 1st-order PT to the A-type structure. It must be noted that some PTs for RE-SOs with a small RE ionic radius have yet to be reported. Besides, a pressure-induced PT to the Gd_2S_3 structure has been found from some C- and B-type RE-SOs at HT. Finally, we must comment that HP studies on trigonal A-type RE-SOs are quite scarce and do not allow us to conclude which is the typical HP phase of A-type RE-SOs. Consequently, more work has to be done in A-type RE-SOs, either studying C- or B-type RE-SOs at higher pressures or studying in better detail RE-SOs crystallizing in the A phase at room conditions, in order to understand the behavior of the trigonal structure and its pressure-induced PTs.

2.2. Group-13 Sesquioxides

Group-13-SOs are highly interesting compounds, due to their chemical and physical properties, which enable their application as catalyst, lasers and light emitting materials [84]. HP studies in group-13-SOs have been conducted on the five compounds. Al_2O_3, also known as alumina, is by far the most studied compound [85–99], followed by In_2O_3 [100–109], Ga_2O_3 [107,110–114], and B_2O_3 [115–121]. Finally, Tl_2O_3 has been the least studied compound [122].

The interest in alumina comes from its high stability, making it interesting for HP science applications, especially as windows in shockwave experiments [123]. However, its main application occurs when alumina is doped with a small amount of Cr^{3+}. Al_2O_3:Cr^{3+}, also known as ruby, presents fluorescence lines that are pressure-dependent and is used as a pressure standard in static HP experiments using anvil cells [124]. Corundum (α-Al_2O_3) is a mineral of alumina that is found in abundance in the earth mantle incorporated into enstatite ($MgSiO_3$) [99]. Given that both minerals might adopt similar structures at ultra-HPs, their study is interesting from a geophysical point of view. In fact, the most stable phase of alumina at room conditions is the corundum structure (s.g. $R\bar{3}c$), where coordination of all Al atoms is six-fold and of O atoms is four-fold [94]. The unit cell has two formula units, with O atoms forming a slightly distorted, hexagonal, close-packed structure [88,125]. The same structure is also found in other SO minerals, such as hematite (Fe_2O_3), eskolaite (Cr_2O_3), karelianite (V_2O_3), and also Ti_2O_3 and Ga_2O_3 [125]. In this structure, cations occupy positions (0, 0, z) and oxygens occupy positions (x, 0, $\frac{1}{4}$) and, if both z and x coordinates were 1/3, the corundum-type structure would have a perfect hexagonal close-packed packing [125].

β-Al_2O_3 is another very interesting polymorph of alumina from a technological application point of view. This material is a non-stoichiometric compound ($Na_2O_x \cdot Al_2O_3$, $5 \leq x \leq 11$) and not a simple variation of alumina [126,127]. Due to its layered crystalline structure, β-Al_2O_3 has a high ionic conductivity and has been studied for solid state battery applications [126,127]. We have not found any HP study of this material.

Theoretical studies of corundum predicted a pressure-induced PT to the Rh_2O_3-II structure (s.g. *Pbcn*) between 78 and 91 GPa [87,92,96,98] and a second PT to an orthorhombic perovskite (Pv) structure (s.g. *Pbnm*) at 223 ± 15 GPa [87,92,96,98,128]. Other theoretical studies predicted that the post-perovskite (PPv) $CaIrO_3$-type structure (s.g. *Cmcm*) would be more stable than the Pv structure at pressures higher than 150 GPa [85,99,129]. However, RT measurements performed up to 175 GPa under hydrostatic and non-hydrostatic conditions showed no PT [88,89]. The PT to the Rh_2O_3-II structure was only observed at HP (>95 GPa) and HT (>1200 K) [86,97] once the energy supplied by temperature allows the overcoming of the kinetic barrier of this 1st-order PT [86,89,96,97,128]. The Rh_2O_3-II structure is directly related to corundum structure; nevertheless, it presents a great distortion in the AlO_6 octahedron [97]. Lin et al. reported that the Rh_2O_3-II-type Al_2O_3 (Cr^{3+} doped) remains stable up to 130 GPa and 2000 K [97]. However, studies using shock waves have shown that a decrease by one order of magnitude in resistivity occurs at 130 GPa [123] that it is coincident with an increase in the density of Al_2O_3 [130], thus indicating a possible PT. This hypothesis was supported by the discovery of a PPv $CaIrO_3$-type polymorph of Fe_2O_3 [131] and $MgSiO_3$ [132]. In 2005, Oganov and Ono were finally able to synthesize the PPv $CaIrO_3$-type phase of Al_2O_3 at ~ 170 GPa and 2500 K [94,129]. They showed that the Rh_2O_3-II → $CaIrO_3$-type PT is a 1st-order PT with ~ 5% of volume decrease [94,129]. The possibility of obtaining this structure at HP and HT was important to understand the physical properties of the elements present in the D″ layer of the earth mantle [129]. This layer is basically composed of a solid solution of $MgSiO_3$, Fe_2O_3 and Al_2O_3. Since, under the HP and HT conditions of the Earth mantle, all these materials are isostructural, their solubility may be facilitated [94].

When synthesized as nanoparticles smaller than 20 nm, alumina tends to crystallize into a cubic structure known as a phase γ (s.g. $Fd\bar{3}m$) [133]. HP experiments at room temperature observed an amorphization of γ-Al_2O_3 around 5 GPa [133]. On the other hand, it was also observed that the γ-Al_2O_3 → $R\bar{3}c$ PT, which occurs at RP near 1473 K, decreases to ~ 1023 K when γ-Al_2O_3 is pressurized at

1 GPa [134]. In addition, HP-HT experiments have revealed other phases of alumina, like polymorphs of RE-SOs B- and C-type, as well as polymorphs λ and μ [135,136]; however, no HP studies on these phases have been reported to our knowledge.

The search for new high hardness materials, such as Al_2O_3, has attracted the attention of many research groups for SOs, including indium oxide (In_2O_3) and gallium oxide (Ga_2O_3) [106]. In_2O_3 is a semiconductor with high potential for many transparent oxide applications, including touch and photovoltaic devices, thermoelectric and gas sensors [137]. At room conditions, In_2O_3 crystallizes in the cubic bixbyite structure (s.g. $Ia\bar{3}$), also known as the C-type RE-SO structure (c-In_2O_3) [106]. In this structure there are two types of In atoms (they are surrounded by oxygen in the octahedral and trigonal prismatic coordination) located at positions 8*b* and 24*d* and one type of O located at position 48*e* [138]. In the 1960s, a PT from c-In_2O_3 to a metastable corundum-like rhombohedral phase (rh-In_2O_3; s.g. $R\bar{3}c$) was reported at HP and HT (6.5 GPa and 1000 °C) [106,139,140]. This PT was also observed through shockwave compression experiments between 15 and 25 GPa [141]. Some HP-XRD studies of both bulk and nanoparticle samples claimed that the c-In_2O_3 → rh-In_2O_3 PT occurs at RT when the sample is exposed to pressures between 12 and 25 GPa [103,104]. This result is controversial since other studies using HP-XRD and HP-RS measurements did not clearly observe this PT up to 30 GPa [100,101]. On the other hand, García-Domene et al. reported that bulk c-In_2O_3 actually undergo a PT to an Rh_2O_3-II-type structure (o1-In_2O_3; s.g. *Pbcn*) orthorhombic phase at pressures above 31 GPa at RT [101]. This structure was also obtained at 7 GPa after laser heating at 1500 °C [106]. This result is consistent with the prediction of theoretical calculations that the Rh_2O_3-II-type phase is the most stable In_2O_3 structure between 8 GPa and 36 GPa [101]. On top of that, looking for a possible $CaIrO_3$-type PPv phase in In_2O_3, Yusa et al. observed another PT from Rh_2O_3-II-type to α-Ga_2S_3-type structure (s.g. *Pnma*) above 40 GPa and 2000 K [107]. A reduction of 7%–8% in volume was observed, unlike the reduction of 2% expected for a Rh_2O_3-II-type → $CaIrO_3$-type transition [107].

Releasing the pressure after obtaining the Rh_2O_3-II-type structure in In_2O_3, García-Domene et al. demonstrated that, at 12 GPa, o1-In_2O_3 undergoes a PT to a previously unknown phase [101]. The combination of experimental and theoretical results helped to conclude that, upon decreasing the pressure to 12.1 GPa, the In_2O_3 recrystallizes in a distorted bixbyite-like structure (o3-In_2O_3; s.g. *Pbca*), isostructural to Rh_2O_3-III [101,108]. Decreasing the pressure below 1 GPa, o3-In_2O_3 undergoes another PT to the metastable rh-In_2O_3 structure. The metastable rh-In_2O_3 phase at room conditions remains stable up to 15 GPa and above this pressure shows a reversible PT to o3-In_2O_3, which is stable up to 25 GPa [101]. The observation of the *Pbca* phase took place only when decreasing pressure using original bulk c-In_2O_3 samples was related to kinetic barriers in the c-In_2O_3 → o3-In_2O_3 PT, that cannot be overcome at RT during upstroke [101]. Similar studies in c-In_2O_3 nanoparticles performed up to 44 GPa did not clearly show these PTs [100,104,105]. Qi et al. reported that, when compressing 6 nm c-In_2O_3 nanoparticles, an irreversible PT to the rh-In_2O_3 phase occurs between 20–25 GPa [104]. Nowadays, it is now possible to synthesize In_2O_3 nanoparticles at room conditions with the rh-In_2O_3 metastable phase at relatively low temperatures (250 to 500 °C) [142–144]. Sans et al. studied rh-In_2O_3 nanoparticles (10–30 nm) up to 30 GPa using XRD and RS measurements [109]. XRD measurements did not show any PT up to 30 GPa, but RS measurements showed peaks of the o3-In_2O_3 phase above 20 GPa [109]. One reason for this discrepancy was attributed to the sensitivity of RS measurements to local structural changes, which is responsible for the observation of PTs at lower pressures in RS compared to XRD measurements [109]. Another reason might be related to the use of less hydrostatic pressure-transmitting medium in RS (MEW) than in XRD (Ar) measurements [109].

Regarding Ga_2O_3, its most stable structure at room conditions is the monoclinic phase (s.g. *C2/m*), known as β-Ga_2O_3 [145,146]. However, depending on the pressure, temperature and atmosphere conditions, it is possible to find Ga_2O_3 in the α, β, γ, σ and ε phases [111,147]. Compared to Al_2O_3 and In_2O_3, HP studies on Ga_2O_3 are scarcer. In 1965, Remeika and Marezio reported the synthesis of α-Ga_2O_3 (s.g. $R\bar{3}c$), which is isostructural to α-Al_2O_3, by pressurizing β-Ga_2O_3 to 4.4 GPa, after heating to 1000 °C and quenching to room conditions [147]. Lipinska-Kalita et al. reported that, upon

pressing nanoparticles (~15 nm) of β-Ga_2O_3 homogeneously dispersed in a host silicon oxide-based glass matrix, it is possible to observe a PT to α-Ga_2O_3 at 6 GPa [111]. In that study, the β-Ga_2O_3 → α-Ga_2O_3 PT is not completed up to 15 GPa and it is not clear whether the PT is induced by glass matrix densification or is an intrinsic behavior of the β-Ga_2O_3 nanoparticles [111]. This work led Machon et al. to study the behavior of β-Ga_2O_3 microparticles by XRD and RS measurements with different pressure-transmitting media [113]. They observed a PT to the α phase above 20 GPa, unlike what was observed in reference [111]. A highly disordered α-Ga_2O_3 was recovered at RP after a fast decompression from 25 GPa and a mixture of α and β phases were recovered when decompression was performed slowly [113]. The β-Ga_2O_3 → α-Ga_2O_3 PT can be considered to be of 1st-order and involves a change in O^{2-} ions packing from cubic to hexagonal, accompanied by a change in Ga^{3+} coordination from four to six [111,113,148].

The β-Ga_2O_3 → α-Ga_2O_3 PT was not clearly observed in an experiment performed up to 65 GPa without pressure-transmitting medium [106]. Instead, XRD measurements at 65 GPa showed only a diffraction pattern similar to a material with low crystallinity or amorphous. After laser heating (~2300 K), a recrystallization to an orthorhombic phase Rh_2O_3-II-type (s.g. *Pbcn*) was observed [106]. This phase remained stable up to 108 GPa and 2500 K. During decompression, the Rh_2O_3-II-type → α-Ga_2O_3 PT was observed between 32 and 21 GPa, being the α phase metastable at RP [106]. These results differ from other published by Lipinska-Kalite et al. up to 70 GPa with (N_2) and without pressure-transmitting medium [110]. In that study, a β-Ga_2O_3 → α-Ga_2O_3 PT was clearly observed, which starts at 6.5–7.0 GPa (3 GPa) and completes at 40 GPa (30 GPa) when measured with (without) pressure-transmitting medium [110]. Through XRD measurements, Lipinska-Kalita et al. observed no evidence of pressure-induced amorphization or deterioration of the diffractogram up to 70 GPa [110]. The β-Ga_2O_3 → α-Ga_2O_3 PT was also observed at 16 GPa in shockwave experiments [149]. Wang et al. conducted HP studies on β-Ga_2O_3 nanoparticles (14 nm) at RT and found the PT to α-Ga_2O_3 above 13.6 GPa [114]. Above this pressure, the α phase remains stable up to 64.9 GPa and stays metastable upon returning to RP [114].

Boron sesquioxide (B_2O_3) is one of the most important oxides in applications involving vitreous systems. In glass form, B_2O_3 has a low melting point (750 K) and a structure similar to vitreous SiO_2 and H_2O [117]. When pressing the glassy material, it is possible to observe a structural rearrangement around 3 GPa that was considered a low- to high-density vitreous PT [118]. Furthermore, starting from the glassy material, it is possible to obtain B_2O_3 crystals at HP and HT. At room conditions, the most stable structure of B_2O_3 is a trigonal structure (s.g. $P3_121$) known as B_2O_3-I, where B is in the center of triangles of O atoms [115–117,119,121]. Despite its stability at room conditions, working with this material is not simple due to its strong hygroscopic behavior, capable of decomposing the sample in a few minutes [121]. Above 3.5 GPa and 800 K, B_2O_3-I undergoes a PT to an orthorhombic structure, known as B_2O_3-II (s.g. $Ccm2_1$), composed of distorted BO4 tetrahedra [116,120]. The B_2O_3-I → B_2O_3-II transition leads to an increase of B and O coordination from 3 to 4, and from 2 to an intermediate between 2 and 3, respectively, and a volume change of ~27% [117,120,150].

The last group-13-SO is thalium oxide (Tl_2O_3). This material is very interesting from a technological point of view as it has potential for interesting applications such as solar cell electrode, optical communication and HT superconductors [151–154]. Its most stable phase at room conditions is c-Tl_2O_3, a bixbyite body-centered cubic phase isostructural to c-In_2O_3. A corundum-like structure (s.g. $R\bar{3}c$) was also observed at HP (6.5 GPa) and HT (500-600 °C) [140]. So far, only one paper reports the properties of the c-Tl_2O_3 at HP, probably due to the toxicity of this material [122]. Theoretical calculations predict a c-Tl_2O_3 → Rh_2O_3-II-type (s.g. *Pbcn*) PT at 5.8 GPa and a second Rh_2O_3-II-type → α-Gd_2S_3-type (s.g. *Pnma*) PT at 24.2 GPa [122]. However, ADXRD measurements at RT, performed using MEW as pressure-transmitting medium, showed only an irreversible pressure-induced amorphization at 25.2 GPa, which was a consequence of kinetic barriers that cannot be overcome at RT [122]. In addition, theoretical calculations predicted a mechanical instability of c-Tl_2O_3 above 23.5 GPa [122]. Future work involving HP and HT is needed to better understand the behavior of Tl_2O_3 at HP.

To finish this section, we summarize in Table 2 the phase transition pressures observed in group-13-SOs.

Table 2. Experimental data of the phase transition pressures (in GPa) for group-13 sesquioxides. The letters A, B, C, D, E, F, G, H, and I refer to the structures $R\bar{3}c$, Rh_2O_3-II-type, $CaIrO_3$-type, $Ia\bar{3}$, $\alpha-Ga_2S_3$-type, $Pbca$, $C2/m$, $P3_121$, and $Ccm2_1$, respectively. Between parentheses are the transition temperatures (when necessary). SW stands for shockwave experiments and NP for nanoparticles.

	$P_{A\to B}$	$P_{A\to C}$			Reference
Al_2O_3	95 (1200 K)				[86]
	96 (>2000 K)				[97]
		150 (>1500 K)			[94]
		170 (2500 K)			[127]
	$P_{D\to A}$	$P_{D\to B}$	$P_{B\to E}$	$P_{B\to F}$	
In_2O_3	6.5 (1273 K)				[140]
	15–25 (SW)				[141]
		31			[101]
		7 (>1700 K)			[106]
			40		[107]
				12	[101]
	$P_{G\to A}$	$P_{G\to B}$			
Gd_2O_3	4.4 (1273 K)				[147]
	20–29				[113]
	16 (SW)				[149]
	16.4–39.2 (NP)				[114]
		65 (2300 K)			[106]
B_2O_3	$P_{H\to I}$				
	3.5 (800 K)				[116,120]
Tl_2O_3	$P_{D\to A}$				
	6.5 (>720 K)				[140]

2.3. Transition-Metal Sesquioxides

TM-SOs belong to a highly heterogeneous family of compounds, as their fundamental (electronic, magnetic) properties strongly depend on the number, and therefore on the spin state, of *d* electrons in the A^{3+} cation. TM-SOs include, among others, the ubiquitous ferric oxide (Fe_2O_3), the commonly-used green pigment Cr_2O_3, or the relatively rare Ti_2O_3 oxide, found in the famous Allende meteorite as the mineral tistarite [155]. Thus, each of these compounds has its own particularities and, regarding the HP structural properties, its specific behavior upon compression.

Among all the TMs, excluding the *f*-block lanthanide and actinide series and including group-3 and group-12 elements, in this section we will only consider A_2O_3 compounds with at least one *d* electron. Thus, Sc_2O_3, Y_2O_3 and La_2O_3 are not included here, since they have been discussed together with the RE-SOs in Section 2.1. Among the rest of possible TM-SOs, only the following compounds have been found to be stable at room conditions: Ti_2O_3, V_2O_3, Cr_2O_3, Mn_2O_3, Fe_2O_3, Co_2O_3, Ni_2O_3, Rh_2O_3 and Au_2O_3. Other compounds, like Hf_2O_3 and Zr_2O_3, might be metastable at HP [156].

With the exception of Mn_2O_3, the most stable form of all TM-SOs at room conditions corresponds to the rhombohedral structure of the corundum. As can be seen in Figure 4a, the lattice parameters of the corundum-like structure adopted by most of TM-SOs are barely reduced by increasing the number of *d* electrons in the A^{3+} cation. This result simply reflects the slight reduction in the atomic radius of the cations with increasing atomic number. However, as can be seen in Figure 4b, the *c*/*a* ratio of these compounds displays a well-known anomaly around Ti_2O_3 and V_2O_3 that deserves further attention. In particular, V_2O_3 has highly remarkable properties and behaves, upon compression, in a highly

different fashion than other corundum-type TM-SOs [157]. In turn, Mn_2O_3 crystallizes in the so-called bixbyite structure (s.g. 206, $Ia\bar{3}$), which takes the name of the mineral form of Mn_2O_3. The absence of the corundum structure in Mn_2O_3 at room conditions has been attributed to the Jahn-Teller distortion associated with the d^4 Mn^{3+} ion [158].

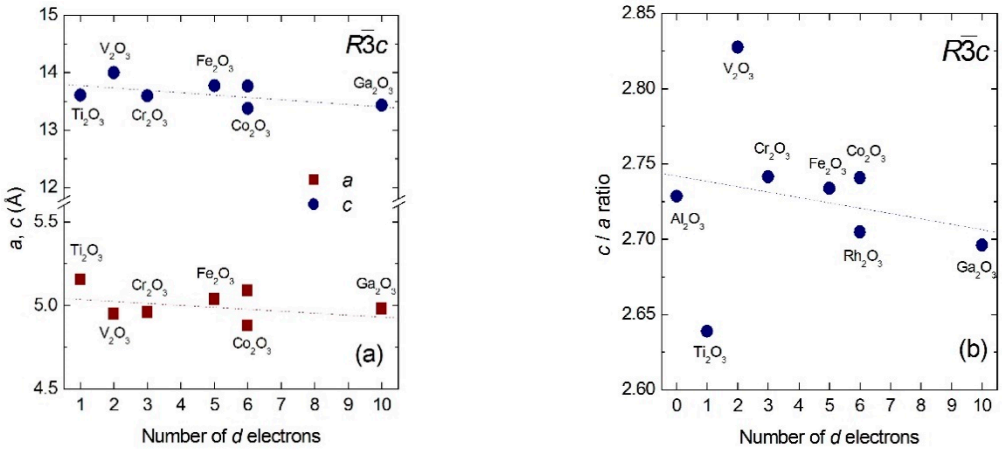

(**a**) (**b**)

Figure 4. (**a**) Lattice parameters, a and c, of different corundum-type 3d-TM-SOs. The plot shows the similarity between the lattice parameters of these compounds. Corundum-type Ga_2O_3 (with 10 d electrons) is also included. (**b**) c/a ratio for different corundum-type TM-SOs. Al_2O_3 (with no d electrons) and Ga_2O_3 (with 10 d electrons) are also included. Note the well-known anomaly around Ti_2O_3 and V_2O_3.

Most TM-SOs have also been found to exhibit other stable or metastable polymorphs at room conditions, as well as at HP. Next, we focus on the rich and varied HP behavior of the different phases of TM-SOs, with special emphasis on Fe_2O_3, Mn_2O_3 and V_2O_3.

Iron oxides are highly important materials in a large variety of disciplines, including materials science, geology, mineralogy, corrosion science, planetology and biomedicine. In the particular case of iron SO (iron (III) oxide or ferric oxide), there exist several polymorphs that are stable or metastable at room conditions: α, β, γ, ε and ζ. First, we will briefly describe these phases at room conditions and, afterwards, we will discuss their HP behavior.

The most common phase of Fe_2O_3 is the α phase, which has the corundum structure and is ubiquitously found in nature as the mineral hematite. α-Fe_2O_3 is a wide-gap antiferromagnetic insulator, with a Morin transition around 250 K. It is weakly ferromagnetic from this temperature up to a Néel temperature around 950 K, above which it becomes paramagnetic. Besides temperature and doping, pressure is a highly convenient tool to modify the insulating/metallic state of this type of material. In particular, hematite can be considered as an archetypal Mott insulator [159] and is interesting from the point of view of metal-insulator PTs in highly correlated electron systems.

The mineral hematite is the main ore of iron and a very common phase in sedimentary rocks, where it occurs as a weathering or alteration product. It is, however, unlikely that Fe_2O_3 or any of its HP phases have much relevance in the Earth's lower mantle, where Fe^{3+} is mainly incorporated into other minerals, like bridgmanite or garnet, with the possible coexistence of reduced iron-rich metal (Fe^0) [160]. In contrast, it cannot be ruled out that Fe_2O_3 may be responsible for the presence of magnetic anomalies in the upper mantle arising from deep-subduction processes [161]. Thus, the HP behavior of hematite may still be highly relevant from a geophysical point of view, as it might play a key role in relation to the magnetic properties of recycled crust materials in subduction zones.

The γ phase of Fe_2O_3 is also found in the Earth's crust as the relatively common mineral maghemite, which is formed by weathering or low-temperature oxidation of magnetite and related spinel minerals. Maghemite, which is also a very common corrosion product, is metastable and transforms upon

heating into the α phase. γ-Fe_2O_3 has the same cubic spinel ferrite structure (s.g. 227, $Fd\bar{3}m$) as magnetite ($Fe^{2+}Fe^{3+}{}_2O_4$), with 1/3 of Fe atoms tetrahedrally coordinated with oxygen (A sites), and 2/3 octahedrally coordinated with oxygen (B sites). Thus, maghemite can be considered as a Fe^{2+}-deficient magnetite, with all A sites filled with Fe^{3+} and only 5/6 of the total available B sites filled with Fe^{3+}; i.e., with 1/6 of vacant (V) B sites, so it can be noted as $(Fe^{3+})^A(Fe^{3+}{}_{5/3}V_{1/3})^BO_4$. γ-$Fe_2O_3$ exhibits soft ferrimagnetism at RT, with a Curie temperature around 950 K [162]. Most remarkably, ultrafine particles of γ-Fe_2O_3 exhibit super-paramagnetism, which is related to the thermally induced random flip of the magnetization in ferromagnetic nanoparticles. This phase is being intensively investigated in order to construct an appropriate theoretical framework for this phenomenon, which might set a limit on the storage density of hard disk drives.

A rare orthorhombic polymorph of Fe_2O_3, named ε-Fe_2O_3 (s.g. 33, $Pna2_1$), has also been found to be stable at room conditions. This phase seems to exist only in nanosized form and was first reported back in 1934 [163]. A few years later, it was synthesized and characterized by Schrader et al. [164]. The crystal arrangement of ε-Fe_2O_3 is considered as intermediate between the structures of the α and γ phases, with three octahedral FeO_6 units (two of which are distorted) and a FeO_4 tetrahedral unit. It is worth noting that this phase has recently been found in nature as the Al-bearing nanomineral luogufengite, which is an oxidation product of Fe-rich basaltic glass at HT [165]. It has also been found in ancient black-glazed wares from Jianyang county, China, produced during the Song dynasty (960–1279 AD) [166]. Recent studies have also shown that this polymorph is a non-collinear ferrimagnet [167]. Owing to its remarkable magnetic properties, such as giant coercive field, ferromagnetic resonance and magnetoelectric coupling [168], this phase is highly promising to develop a broad range of novel applications. Besides, the giant coercive field of lougufengite might explain the observed high-remanent magnezitation in some igneous and metamorphic rocks [169].

In contrast to ε-Fe_2O_3, β-Fe_2O_3 and the recently discovered "ζ-Fe_2O_3" phase [170] have not been found to occur in nature so far. These two rare polymorphs are metastable phases that have been obtained by synthetic methods and which only exist in nanocrystalline form. The beta phase exhibits the bixbyite structure, with trivalent Fe ions occupying two non-equivalent octahedral sites. It exhibits paramagnetic behavior at room conditions, with a Néel temperature just above 100 K. Antiferromagnetic ordering is observed below this temperature. Upon heating, β-Fe_2O_3 undergoes a PT to either the α or γ phases. In turn, "ζ- Fe_2O_3" displays a monoclinic structure (s.g. 15, $I2/a$) and was obtained by applying HP (>30 GPa) to β-Fe_2O_3 [169]. Surprisingly, this new phase (with a Néel temperature around 70 K) is metastable after releasing pressure, being able to withstand pressures up to ~70 GPa.

In spite of much effort to elucidate the structural, magnetic and electronic properties of α-Fe_2O_3 (hematite) at HT and HP [159,170–176], the HP behavior of the most important phase of Fe_2O_3 is still under debate. Only recently was a complete T-P phase diagram of α-Fe_2O_3 established [176]. According to that work, α-Fe_2O_3 transforms at RT to a HP phase above ~50 GPa, with an ~8.4% volume discontinuity. It is worth noting that in this work the HP phase was called "ζ-phase" and was indexed as triclinic ($P\bar{1}$) [175]. This phase is not equivalent to the monoclinic s.g. $I2/a$ phase stable at room conditions, also named "ζ-Fe_2O_3", which was produced by Tucek et al. [169]. It must be noted that the $P\bar{1}$ phase was previously indexed as monoclinic ($P2_1/n$) in reference [175]. The fact that this HP phase is relabeled as "double perovskite" in reference [170] and treated as s.g. $P2_1/n$ only adds confusion to the nomenclature of the different phases of such an important compound as Fe_2O_3.

As already mentioned, the single-crystal diffraction patterns of the $P\bar{1}$ HP phase were initially indexed in a monoclinic unit cell [173], but were subsequently refined into a triclinic s.g. $P\bar{1}$ structure [175]. However, previous works had assigned the HP phase (~50 GPa) of hematite to either a distorted corundum phase (Rh_2O_3-II-type structure, s.g. $Pbcn$) [159,170,172,177] or to a Pv structure (s.g. $Pbnm$) [129,178]. According to reference [175], the $P\bar{1}$ structure of Fe_2O_3 is closer to a distorted (and not "double", as in reference [176]) Pv structure. However, a more recent study up to ~79 GPa has put into question the very existence of the distorted Pv phase [174], in agreement with

previous results [179]. The data and analysis of reference [159] indicate that the 1st-order PT around 50 GPa is accompanied by an insulator-to-metal transition with collapse of the magnetic properties. The structural PT would thus be very progressive [160,170], starting from the corundum-type structure and leading to a distorted Rh_2O_3-II-type structure. In contrast, Bykova et al. suggested that the Rh_2O_3-II-type structure only occurs below 50 GPa at HT and would be reconstructive, with a volume change of ~1.3% [173]. According to this work, the distorted Pv phase shows a PT at RT around ~67 GPa to a possibly metastable orthorhombic structure (s.g. 41, *Aba2*) or to a $CaIrO_3$-type PPv phase (s.g. *Cmcm*) [175]. In fact, the *Aba2* to PPv PT was observed at HT (above 1600 K). After quenching the samples to RT, the PPv polymorph was found to be stable up to 100 GPa and down to 26 GPa; however, hematite was recovered below this pressure. In turn, the metastable *Aba*2 phase seems to be preserved at 78 GPa, up to 1550 K. This polymorph, also observed by Greenberg et al. [176] at RT, can be considered as a metastable HP phase at low temperature. It adopts a similar packing to the Rh_2O_3-II-type structure observed at low pressures, but, instead of octahedra, it consists of FeO_6 prisms. Recent results obtained by Sanson et al. are compatible with the existence of the *Aba*2 polymorph [174]. However, these authors seem to rule out not only the $P2_1/n$ HP phase, but also the *Pbnm* one.

Regarding the PPv structure, Ono et al. had previously reported a PT from hematite to the PPv structure above 30 GPa at HT [131]. Moreover, a new phase was found above 50 GPa to an unknown phase that was tentatively assigned to an orthorhombic or a monoclinic lattice. In relation to the magnetic and electronic properties of this phase, Shim et al. showed that the magnetic ordering of PPv-type Fe_2O_3 is recovered after laser heating at 73 GPa [179]. According to these authors, the appearance of the PPv phase gives rise to the transformation of Fe^{3+} ions from a low-spin to a high-spin state, with Fe_2O_3 undergoing a semiconducting-to-metal PT. This effect might be relevant to understand the electromagnetic coupling between the Earth's mantle and the core. Previous research had already investigated with Mössbauer spectroscopy the high-spin to low-spin PT in α-Fe_2O_3, at HP associated to the structural PT [180,181].

Indeed, one of the main interests of studying hematite at HP, besides its crystal structure and phase diagram, has to do with its electronic properties and the nature of the HP-PT [171]. What drives the HP-PT in hematite? Is it the crystal structure, or the electronic structure? Note that one could expect that electronic PTs, such as the insulator-metal Mott PT observed at 50 GPa [159] or the high-spin to low-spin PT, are isostructural. According to this argument, the PT observed in hematite at ~50 GPa, accompanied by a large volume change, should drive the change in electronic properties. Badro et al. reached this conclusion and indicated that the electronic PT is isostructural and occurs after the crystal structure PT [171]. However, Sanson et al. have recently reached the opposite conclusion, i.e., that the structural PT is driven by the electronic transition [174]. These authors analyzed the local structure and observed no FeO_6 octahedra distortion at HP, in disagreement with previous works [170]. A careful analysis recently performed by Greenberg et al. suggests that the pressure-induced insulator-to-metal PT in hematite arises from site-selective delocalization of electrons [176]. According to this study, such site-selective Mott transition ought to be characterized by delocalization (i.e., metallization) of Fe 3*d* electrons on only half of the sites in the unit cell. This work suggests that the interplay between crystal structure and electronic correlations may yield a complex behavior that could be also relevant to understand the HP behavior of other TM-SOs.

With regard to the rest of Fe_2O_3 phases stable at room conditions (γ, β and ε), the amount of published works regarding their HP behavior is sizably lower in comparison to hematite. The phase diagram of γ-Fe_2O_3 (maghemite) is relatively simple, since this phase readily transforms to α-Fe_2O_3 around 35 GPa [182]. Therefore, much of the effort regarding this phase has been in relation to the comparison of the compression behavior between bulk and nanocrystalline samples (see reference [183] and references therein). Further details about polymorphic PTs of nanosized Fe_2O_3, including doping, temperature and HP, can be found in reference [184]. In the case of maghemtite, Jiang et al. found that nanocrystalline γ-Fe_2O_3 transforms to hematite at ~27 GPa, below the PT pressure for bulk material [182]. As shown by Zhu et al., the γ-to-α PT might be initiated at the same pressure, around

16 GPa, both in bulk and nanocrystalline forms [183]. According to these authors, vacancies might play an important role in the structural PT. More recently, a combination of XRD and Mössbauer spectroscopy up to 30 GPa on vacancy-ordered maghemite has shown that the γ-to-α PT would be initiated at 13–16 GPa, giving rise to a particular texture in the transformed α-Fe_2O_3 material [185].

Finally, in relation to the Fe_2O_3 polymorphs, we must mention the recent HP study of ε-Fe_2O_3 by Sans et al. [186]. These authors found that this rare nanocrystalline phase, which is a promising magnetic material for a range of technological applications, is stable up to 27 GPa. Above this pressure, evidence for a PT, in which the tetrahedrally coordinated iron ions change towards quasi-octahedral coordination, was observed. Given that this phase has very high magnetic coercivity, it remains to be investigated whether its mineral form may play any relevant role in the magnetic remanence of mantle xenoliths, and in the magnetism of subducting slabs at depths corresponding to the mantle transition zone [161].

Manganese SO (Mn_2O_3) is unique among 3*d*-TM-SOs because its most stable phase at room conditions (α-Mn_2O_3) does not adopt the corundum structure. Instead, it crystallizes in the so-called cubic bixbyite structure that takes the name from the mineral form of this compound. In bixbyite, Mn^{3+} occupies five different crystallographic sites, each of them surrounded by a highly distorted octahedron of O atoms. Such distortion originates from the Jahn-Teller effect, due to the lowering of overall energy as a consequence of a distortion-induced loss of degeneracy in the 3*d*-orbitals of the sixfold-coordinated Mn^{3+} ions. As discussed by several authors, the Jahn-Teller distortion might explain the fact that Mn_2O_3 does not adopt the corundum structure at room conditions [158]. Also, it has been predicted that HP might suppress the Jahn-Teller effect, which would make Mn_2O_3 transform to a corundum-type polymorph and, afterwards, follow the usual sequence of pressure-induced PTs observed in the rest of TM-SOs [140]. α-Mn_2O_3 has been shown to be antiferromagnetic, with a Néel temperature of around 79 K [187] and has recently attracted considerable interest due to its potential use in chemical catalysis and magnetic devices, and also for energy conversion and storage applications.

Interestingly, the bixbyite structure actually occurs in doped samples and/or at temperatures slightly above RT. Indeed, it has been shown that Mn_2O_3 undergoes a subtle cubic-to-orthorhombic (*Pcab*) PT around RT and that the bixbyite structure is stabilized by the presence of impurities [188]. The low-temperature phase *Pcab* is just an orthorhombically distorted bixbyite structure. There exists another polymorph of Mn_2O_3 stable at room conditions, namely γ-Mn_2O_3. It is a tetragonal spinel-like polymorph (s.g. $I4_1/amd$), related to Mn_3O_4. This phase, which is ferrimagnetic below 39 K, can be viewed as the equivalent of maghemite in the case of the Fe_2O_3 system.

Several studies have investigated the HP phases of Mn_2O_3 [140,189–194]. It is now clear that α-Mn_2O_3 transforms at RT to a $CaIrO_3$-type PPv-like structure above 16 GPa [190–194] with a large volume collapse of ~12%. Thus, no Pv polymorph is observed between the bixbyite and PPv structures at RT. As pointed out by Santillán et al. [190], this might be due to the similarity between the two structures (cubic bixbyite and PPv). Yamanaka et al. also reported a monoclinic HP phase of Mn_2O_3 that has not been confirmed by any other study [189]. More recently, synthesis performed with a multianvil apparatus and subsequent study of the recovered material has shown that, at HTs (between ~850 and 1150 K) the Pv structure, also called ζ-Mn_2O_3, can be synthesized and recovered at room conditions [193]. This polymorph is formed by a Pv octahedral framework with strongly tilted MnO_6 octahedra. Its crystal structure was determined within the $a = 4a_p$ supercell, s.g. $F\bar{1}$ (s.g. $P\bar{1}$ in the standard setting, see reference [193]), where Mn cations are preferentially found in different sites depending on their valence state (Mn^{2+}, Mn^{3+}, Mn^{4+}). This phase has been shown to be a narrow and direct bandgap semiconductor (0.45 eV) with remarkable hardness [195], and to exhibit a 3:1 charge ordering between two different sites, and a unique orbital texture involving a remarkable alternation of orbitals states [196].

A corundum-type polymorph of Mn_2O_3 (ε-Mn_2O_3) was also recovered at room conditions after applying intermediate pressures (15 GPa) and HT (> 1200 K) [193]. This phase, which is about 1% denser than the bixbyite polymorph, seems to confirm the existence of the undistorted, corundum-type

structure in the exotic Mn_2O_3. It should be noted that, in contrast to this phase and the ζ phase, the more usual HP PPv polymorph is not quenchable at room conditions. The multianvil apparatus experiments also show that reduction of Mn_2O_3 to Mn_3O_4 is observed below 12 GPa at HT (>1200 K) [193]. No HP studies of ε and γ phases are available to our knowledge.

Among TM-SOs, vanadium oxide (V_2O_3) is one of the most interesting materials both from fundamental and applied points of view, due to its remarkable electronic and magnetic properties. This compound has a very rich phase diagram at RP and is often considered a paradigmatic example of metal to Mott-insulator transition in strongly correlated materials. Depending on temperature and doping with small amounts of Cr or Ti, V_2O_3 exhibits different phases including a paramagnetic metallic state, a paramagnetic insulating state or a low-temperature antiferromagnetic insulating state [197,198]. V_2O_3 adopts a corundum-type structure at atmospheric conditions and is found in nature as the rare mineral karelianite, first found in glacial boulders from the North Karelia region, in Finland. A metastable polymorph of V_2O_3 with bixbyite structure was obtained by synthetic methods [199]. This phase transforms into the stable corundum phase above 800 K, and is found to exhibit a paramagnetic to canted antiferromagnetic transitions at about 50 K.

The application of HP strongly modifies the phase diagram of corundum-type V_2O_3. Several studies have investigated the Mott-insulator transition in V_2O_3 and Cr-doped V_2O_3 at HP with a range of different experimental techniques [200–205]. Here, we would like to first focus on the link between the structural and electronic properties of V_2O_3. In particular, McWhan and Remeika [200] studied V_2O_3 and $(V_{0.96}Cr_{0.04})_2O_3$ samples and found that the metallic state typically found in undoped V_2O_3 is recovered by compressing the Cr-doped sample. These authors also showed that the *c*/*a* ratio of the trigonal lattice is related to the insulating/metallic state as a function of Cr-doping level and as a function of pressure. In particular, they found that the *a* parameter of their Cr-doped sample, which was larger than that of undoped V_2O_3 at RP, dropped to the value of V_2O_3 at 4 GPa. In contrast, the *c* parameter was found to barely increase at HP in both samples, implying a remarkable increase in the *c*/*a* ratio in the Cr-doped sample as the metallic state was approached. In fact, they found a sharp increase in *c*/*a* ratio just at the insulator–metal transition. These authors also showed that undoped V_2O_3 becomes even more metallic at HP, with a suppression of the antiferromagnetic-insulating phase above 0.3 GPa.

More recently, Lupi et al. [198] studied with submicron resolution the Mott-insulator transition in Cr-doped V_2O_3. These authors found that, with decreasing temperature (which yields the antiferromagnetic insulator phase), microscopic domains become metallic and coexist with an insulating matrix. This seems to explain why the paramagnetic metallic phase is a poor metal. They attributed the observed phase separation to a thermodynamic instability around the Mott-insulator transition, showing that such instability is reduced at HP. Therefore, they concluded that the Mott-insulator transition is a more genuine Mott transition in compressed samples, which also exhibited an abrupt increase in the *c*/*a* ratio around the insulator-to-metal transition (i.e., around 0.3 GPa). This result confirms the close relationship between the structural properties of V_2O_3, the nature of the Mott-insulator transition and the role of HP in the modification of the electronic properties of this interesting compound.

In contrast to other TM-SOs, the compression of V_2O_3 is highly anisotropic (the *a* axis is nearly three times more compressible than the *c* axis) [206] and the unusual behavior of the *c*/a ratio is closely related to the Mott-insulator transition. It was also shown that the atomic positions in V_2O_3 tend to those of the ideal hcp lattice at HP, with large changes in interionic distances and bond angles upon compression [206]. Zhang et al. observed a pressure-induced PT to an unknown phase around 30 GPa [207]. Ovsyannikov et al. found two different PTs above 21 GPa and 50 GPa, respectively, and attributed the first HP phase to an Rh_2O_3-II-type orthorhombic structure [157]. With regard to the second HP phase, they conclude that it seems not to be related to the Th_2S_3- and α-Gd_2S_3-type structures predicted by Zhang et al. in V_2O_3, of around 30–50 GPa [208]. In conclusion, more work is needed to unveil the HP behavior of both the corundum and bixbyite polymorphs of V_2O_3.

Besides the compounds discussed above, other TM-SOs have been synthesized and/or exist in nature that crystallize in the corundum-structure at room conditions: the 3*d*-SOs Ti_2O_3, Cr_2O_3, and Co_2O_3, and the 4*d*-SO Rh_2O_3. There are also a few reports about the possible synthesis and characterization at room conditions of hexagonal Ni_2O_3 [209,210] and 5*d*-SO Au_2O_3 [211]. However, more work would be required to unambiguously demonstrate the stability of these two latter compounds at room conditions. Note that no natural occurrence of SOs with Ni or Co ions, both of which are more stable as divalent cations, has been found so far. On the other hand, no HP study is known for Au_2O_3.

The amount of HP investigations on the above mentioned materials is variable. Minomura and Drickammer [212] reported HP resistance measurements on several compounds at RT. They found a resistance maximum around 11 GPa in Ni_2O_3 that could be indicative of a PT. Unfortunately, no additional HP investigations can be found in the literature on this material. In the case of Co_2O_3, Chenavas et al. reported a low spin to high spin transition in quenched material, subject to 8 GPa and 850 °C, from a synthesis process involving different chemical reactions [213]. Therefore, the fundamental properties of both Ni_2O_3 and Co_2O_3 at HP have yet to be fully investigated.

Chromia (Cr_2O_3) is another important TM-SO, both from technological and fundamental points of view. This material with corundum structure occurs in nature as the uncommon mineral eskolaite. However, it is probably better known for its high stability and hardness, which makes it a commonly used green pigment and abrasive material. Cr_2O_3 is a typical antiferromagnetic insulator with a Néel temperature T_N ~307 K, but it is remarkable as it shows an intriguing linear magnetoelectric effect that has attracted some research attention in relation to spintronic applications. Although the existence of HP polymorphs of Cr_2O_3 have not yet been well-established [214,215], it is clear that HP affects the magnetic properties of this compound. For instance, as recently shown by Kota et al., hydrostatic pressure may increase the T_N of corundum-type Cr_2O_3, which could provide an enhancement of the magnetoelectric operating temperature in compressed samples [215]. However, there is an ongoing controversy in the literature in relation to the sign of dT_N/dP (see reference [215] and references therein). With regard to its crystal structure at HP, no PT was found either by Finger and Hazen up to 5 GPa [206], or by Kantor et al. up to ~70 GPa [216]. In contrast, Shim et al. observed several changes around 15–30 GPa on pure synthetic Cr_2O_3 under cold compression that were compatible with a PT to a monoclinic V_2O_3-type (*I*2/*a*) structure [217]. According to these authors, a second PT could occur above 30 GPa at HT. The new HP-HT phase might be explained by either orthorhombic, Pv, or Rh_2O_3-II-type structures. In fact, the orthorhombic Rh_2O_3-II-type phase had been previously predicted to exist at ~15 GPa by first-principles calculations [218]. However, the recent results by Golosova et al. up to 35 GPa, also on synthetic Cr_2O_3, seem to rule out both PTs [219]. While these authors report a somewhat lower $(1/T_N)(dT_N/dP)$ value in relation to reference [215] (0.0091 GPa^{-1} vs. 0.016 GPa^{-1}), their structural data point towards a slight anisotropy in the pressure behavior of the *c*/*a* axis at around 20 GPa, which could be of magnetic origin. Additional work is thus required to fully understand the HP behavior of chromia.

In the case of Ti_2O_3, which can be found in nature as the rare tistarite mineral, HP-XRD studies were first conducted by McWhan and Remeika [200] with the aim of comparing the results obtained for this compound with those of V_2O_3. Later on, Nishio-Hamane et al. reported a PT from corundum-type Ti_2O_3 to an orthorhombic Th_2S_3-type (s.g. *Pnma*) structure above 19 GPa and 1850 K, being the new polymorph metastably recovered at room conditions [220]. The same structure had been previously predicted at ultra HP for the case of Al_2O_3 [221]; hence, the synthesis of the Th_2S_3-type polymorph in Ti_2O_3 has been a remarkable finding, shedding new light on the fundamental properties of the TM-SOs family. In Ti_2O_3, the Th_2S_3-type structure was found to be ~10% denser than the corundum-type phase. Subsequently, Ovsyannikov et al. [222] synthesized polycrystalline Ti_2O_3 samples with Th_2S_3-type structure with the aim of studying its structural stability up to 73 GPa and 2200 K. The HP behavior of the structural, optical and electronic properties of this unusual, golden-colored polymorph of Ti_2O_3 were later thoroughly investigated [223,224], together with the T-P phase diagram of Ti_2O_3 [224].

With regard to 4*d*-SOs, there are a few reports on the existence of such compounds at room conditions, the most relevant of which is Rh_2O_3. Two low-pressure polymorphs of this material are known, namely Rh_2O_3-I and Rh_2O_3-III. While the stable phase at room conditions, Rh_2O_3-I, adopts a corundum-type structure, the Rh_2O_3-III polymorph crystallizes in an orthorhombic *Pbca* structure and is only stable at RP and HT (>750 °C) [225]. In addition, an HP phase, known as Rh_2O_3-II, was synthesized by Shannon and Prewitt at 6.5 GPa and 1200 °C [226]. This phase was found to adopt an orthorhombic *Pbna* structure, similar to that of corundum as it contains RhO_6 octahedra that share their faces. In Rh_2O_3-II, however, only two edges of each octahedra are shared with other octahedra. In spite of the use of HP to synthesize Rh_2O_3-II, only a limited number of HP studies on this phase can be found in the literature. Zhuo and Sohlberg investigated theoretically the stability of this phase in comparison to Rh_2O_3-I and Rh_2O_3-III, which allowed them to predict the phase diagram of Rh_2O_3 [227]. According to their results, Rh_2O_3-II is stable below ~5 GPa and HT (>700 K), while the Rh_2O_3-III form is the main phase above 5 GPa, regardless of temperature. Unfortunately, no experimental HP studies dealing with the structural properties of any of the Rh_2O_3 phases have been published so far. Experimental work on this material, and, in particular, on the Rh_2O_3-III polymorph, due to its connection to the HP phases of other SOs, as described above, is still necessary.

Possible stable forms of other 4*d*-SOs, like Mo_2O_3 and W_2O_3, have been reported in relation to the growth of thin films or coatings (see bibliography in reference [228]). Recent DFT calculations predict that corundum-type Mo_2O_3 might be stabilized at 15 GPa, while a much higher pressure (60 GPa) is obtained by these authors for W_2O_3 [228]. Similar conclusions have been reached by other authors in relation to Hf_2O_3 and Zr_2O_3 using crystal prediction methods [157,229]. These two SOs might be metastable at HP. So far, however, there is no experimental evidence for the existence and stability of these SOs at HP. Much experimental and theoretical effort is still required to understand the stability and behavior of these two SOs upon compression, which could lead to the discovery of new HP phases with remarkable properties.

To finish this section, we summarize in Table 3 the phase transition pressures and HP phases observed in the best studied TM-SOs.

Table 3. Summary of the high pressure (HP) phases and phase transition (PT) pressures, P_T (in GPa) reported for the best studied transition-metal sesquioxides (TM-SO) materials: Fe_2O_3, Mn_2O_3, V_2O_3 and Ti_2O_3. The fourth column shows the resulting phase obtained at HP starting from the phase displayed in the first column (DPv: distorted perovskite; PPv: post-perovskite; LH: laser heating).

Compound	P_T	Temperature	HP Phase	Reference
α-Fe_2O_3 (hematite, $R\bar{3}c$)	54	RT	DPv, $P\bar{1}$	[175]
α-Fe_2O_3 (hematite, $R\bar{3}c$)	67	RT	*Aba*2	
α-Fe_2O_3 (hematite, $R\bar{3}c$)	40	LH	Rh_2O_3-II, *Pbcn*	[173]
α-Fe_2O_3 (hematite, $R\bar{3}c$)	68	LH	PPv, *Cmcm*	
β-Fe_2O_3 ($Ia\bar{3}$)	30	RT	"ζ-Fe_2O_3"	[169]
γ-Fe_2O_3 (maghemite, $Fd\bar{3}m$)	35	RT	α-Fe_2O_3	[182]
ε-Fe_2O_3 (luogufengite, $Pna2_1$)	27	RT	ε'-Fe_2O_3	[186]
α-Mn_2O_3 (bixbyite, $Ia\bar{3}$)	16–25	RT	PPv, *Cmcm*	[190]
α-Mn_2O_3 (bixbyite, $Ia\bar{3}$)	18	800 K	Pv, $P\bar{1}$	[193]
α-Mn_2O_3 (bixbyite, $Ia\bar{3}$)	13	1100 K	ε-Mn_2O_3, $R\bar{3}c$	
V_2O_3 (karelianite, R$\bar{3}c$)	21–27	LH	Rh_2O_3-II, *Pbcn*	[157]
V_2O_3 (karelianite, $R\bar{3}c$)	50	LH	PPv, *Cmcm* (?)	
Ti_2O_3 (tistarite, R$\bar{3}c$)	19	1850 K	Th_2S_3-type, *Pnma*	[220]

2.4. Group-15 Sesquioxides

Group-15-SOs are relevant in a multitude of technological [230–232] and medical [233–235] applications, but the main interest in the study of the properties of these compounds resides in the

physical–chemical interactions of their chemical bonds. The progressive increase in the strength of the stereoactive cationic lone electron pair (LEP) going up along the group 15 column, i.e., as the cation becomes lighter, dominates the formation and compressibility of the resulting crystallographic structures. In other words, the influence of the cation LEP determines the different existing polymorphs of group-15-SOs and it is possible to observe several trendlines of their behavior at HP. According to the literature, the group-15-SO polymorphs can be obtained from a defective fluorite structure where oxygen vacancy arrays are applied along different crystallographic directions [236,237]. These arrays define most of the polymorphs found at room conditions in these SOs. Nevertheless, the crystalline phases formed are quite different from the rest of SOs, mainly due to the above-mentioned influence of the LEP.

Structural phases belonging to the cubic family are observed in group-15-SOs since the most usual structures of arsenic and antimony SO crystallizes in the s.g. $Fd\bar{3}m$. They are obtained by applying an array model along the (111) direction to a defective fluorite structure. They have been experimentally found in c-As_2O_3 (whose mineral form is called arsenolite) and α-Sb_2O_3 (whose mineral form is called senarmontite). These SOs are also noted as As_4O_6 and Sb_4O_6, respectively, because this notation reflects the molecular arrangement of these two molecular or zero-dimensional solids. The molecular units X_4O_6 (X= As, Sb) are disposed in a closed-compact adamantane-type molecular cages, joined together by van der Waals (vdW), and chalcogen bonding among the closest arsenics belonging to different molecular units. In this case, the cations belonging to the same molecular unit form pseudo-tetrahedral units following the same disposition as their counterpart, the white phosphorus (P_4). The molecular cages are stabilized by the cationic LEP oriented towards the outside of the cage, which confers great stability to the molecular unit. The HP behavior of both Sb_4O_6 and As_4O_6 dimorphs is quite different. They undergo different PTs [238–242], and both compounds show a pressure-induced amorphization driven by mechanical instability [238–240]. The origin of this instability is associated with the steric repulsion caused by the increase in the interaction between different molecular units when pressure increases [238]. It has been shown in a HP study using different pressure-transmitting media that the instability is enhanced by the loss of the hydrostatic conditions [241]. However, up to 15 GPa, both compounds behave differently. Whereas two 2nd-order isostructural PTs were observed in Sb_4O_6 at 3.5 and 12 GPa, respectively [242], no pressure-induced PT was reported in As_4O_6 [239,240]. The PTs exhibited by Sb_4O_6 at 3.5 and 12 GPa were suggested to be due to the loss of its molecular character and related to changes in the hybridization of Sb *5s* and O *2p* electrons, i.e., they are related to the decrease in LEP stereoactivity at HP [242].

At 15 GPa, Sb_4O_6 tends to form a new HP structure that can be defined by a distortion of the structural lattice due to the loss of the molecular character [238]. This HP phase crystallizes in a tetragonal structure (s.g. $P\bar{4}2_1c$) similar to that of β-Bi_2O_3 [243] that will be described later. At HP (9-11 GPa) and HT (573–773 K), cubic Sb_4O_6 undergoes a 1st-order PT towards a new polymorph called γ-Sb_2O_3 [244]. This new phase crystallizes in an orthorhombic structure s.g. $P2_12_12_1$, where the trigonal pyramid form given by the coordination of the Sb atom surrounded by O atoms in the cubic phase is changed by a tetrahedral unit in the orthorhombic phase, where the LEP acts as a pseudo-ligand. The tetrahedral units are arranged, forming chains or rods along the *a-axis* that show strong similarities with the β-Sb_2O_3 polymorph (s.g. *Pccn*), whose $(Sb_2O_3)_\infty$ rods are aligned along the *c-axis*. Due to its rod-like structure, orthorhombic β-Sb_2O_3 is a quasi-molecular or acicular solid with two independent rods in the unit cell. In this structure, each Sb atom is bonded to three oxygen atoms, with their LEP oriented towards the void formed by the rod arrangement. Thus, this SO can be described by rods and linear voids oriented along the *c-axis*, being isostructural to the ε-Bi_2O_3 phase [245]. No HP study of ε-Bi_2O_3 is known so far.

HP studies of β-Sb_2O_3 revealed a 1st-order PT around 15 GPa [246,247]. Nevertheless, the nature of its HP phase is still under debate. Zou et al. tentatively assigned it to a monoclinic structure with s.g. $P2_1/c$. β-Sb_2O_3 also shows strong similarities with the tetragonal phase of bismuth SO (named β-Bi_2O_3), which crystallizes in s.g. $P\bar{4}2_1c$ [243]. In fact, β-Bi_2O_3 is a metastable polymorph obtained by heating

the most stable phase of the bismuth SO (α-Bi_2O_3) to 650 °C [248]. This material can be considered a defective fluorite structure, where an (100) array of vacants is applied [236]. This polymorph contains a linear channel, as well as β-Sb_2O_3, with the cation LEP oriented towards the center of this empty channel. β-Bi_2O_3 is very interesting from a physical–chemical point of view because it is a clear example of an isostructural 2nd-order PT. This structure is characterized by a Bi atom located at an 8e Wyckoff site and two O atoms located at 8e and 4d Wyckoff sites, with the Bi atom coordinated to six O atoms, forming a distorted pyramid. Above 2 GPa, several Wyckoff coordinates of β-Bi_2O_3 symmetrize, remaining fixed up to 12 GPa [243]. Thus, the six different Bi-O interatomic distances observed at RP in the polyhedral unit only become three different Bi-O bond lengths, thus reducing the eccentricity of the Bi atom drastically, up to 2 GPa. This PT is even more explicit when analyzing the compressibility of the unit cell volume below and above 2 GPa. Finally, a progressive broadening of the peaks leads to a pressure-induced amorphization above 12 GPa that is completed at 20 GPa [243].

α-Bi_2O_3 crystallizes in a monoclinic s.g. $P2_1/c$ structure, where Bi atoms are located in two inequivalent crystallographic 4e sites and O atoms are located in three inequivalent 4e Wyckoff positions. One of the Bi atoms is penta-coordinated and the other is hexa-coordinated. This polymorph remains in the same structure up to 20 GPa, where a pressure-induced amorphization occurs [249]. The amorphization was explained by a frustrated PT towards the HPC-Bi_2O_3 polymorph, since the HPC-phase is thermodynamically more stable than the α-phase above 6 GPa, according to DFT calculations. This ongoing PT is likely inhibited by the kinetic barriers between both phases. The correlation between the amorphous phase and the HPC polymorph was revealed, thanks to the analysis of the diffraction pattern as a function of the interionic distances, using the process described in reference [250]. Results indicated average interatomic Bi-O distances closer to those of the HPC-Bi_2O_3 than to any other polymorph. HPC-Bi_2O_3 crystallizes in the hexagonal s.g. $P6_3mc$ structure, and it is the HP phase of the HP-Bi_2O_3 phase, above 2 GPa [251]. In turn, HP-Bi_2O_3 with s.g. $P31c$ was obtained from α-Bi_2O_3 at HP and HT (6 GPa and 880 °C) [252]. The strong polymorphism exhibited by Bi_2O_3 does not require the application of HP. It must be noted that α-Bi_2O_3 at HT (above 400 °C) shows a PT to R-Bi_2O_3 (s.g. $P2_1/c$) [252], which, despite belonging to the same s.g. as α-Bi_2O_3, has a completely different structure. No HP study of R-Bi_2O_3 is known.

In the same s.g. $P2_1/n$, related to the α- and R-Bi_2O_3 phases, one can find two additional As_2O_3 polymorphs, whose names are claudetite-I [253] and claudetite-II [254]. The naturally stable phase, claudetite-I, has been only characterized by HP-RS measurements to our knowledge, revealing a possible PT between 7–13 GPa and a lack of pressure-induced amorphization up to 40 GPa [255]. Claudetite-II is a synthesized quasi-layered material, similar to As_4O_6, where the molecular unit is an open shell forming AsO_3E pseudo-tetrahedra (where E denotes the cation LEP) [256]. In this case, the LEPs of neighboring cations are oriented towards opposite neighboring layers. This particular structure shows several pressure-induced 2nd-order PTs around 2 and 6 GPa [257], given by two abrupt breakdowns of inversion centers that lead to doubling and hexaplicating the original unit cell, respectively. Additionally, a PT around 10.5 GPa leads to the non-centrosymmetric HP phase β-As_2O_3 (s.g. $P2_1$).

Another group-15-SO crystallizing in the monoclinic s.g. $P2_1/n$ structure is the phosphorous SO (P_2O_3), which keeps the molecular character of cubic arsenic and antimony SOs, i.e., P_4O_6 [258]. Nevertheless, the symmetric distribution of the different P_4O_6 molecular cages is distorted in the case of monoclinic P_2O_3. The HP study of P_2O_3 exhibits strong difficulties, since it is only stable at low-temperatures, below RT. Thus, the HP behavior of this compound is still unknown.

To finish, we summarize in Table 4 the 1st- and 2nd-order PTs observed in group-15-SOs.

Table 4. Experimental and theoretical (DFT) data of the PT pressures (in GPa) for group-15-SOs. PIA stands for pressure-induced amorphization and MEW for methanol-ethanol mixture.

s.g.	Compound	2nd-Order PT	1st-Order PT	PIA	Technique	Reference
$Fd\bar{3}m$	As_4O_6	-	-	18.7	DFT	[240]
		-	-	15	XRD (MEW)	[239]
		-	-	-	XRD (He)	[241]
	Sb_4O_6	3.5 10			XRD, RS, DFT (MEW)	[242]
		-	25	30	XRD (Ne)	[238]
$P2_1/c$	mII-As_2O_3 (claudetite II)	2	6	11	-	XRD (He)	[256]
	α-Bi_2O_3	-	-	20	XRD, RS, DFT (MEW, Ar)	[249]
	mI-As_2O_3 (claudetite I)	-	-	-	RS	[253]
Pccn	β-Sb_2O_3	7	15	33	XRD, RS (Ne)	[246]
		-	13.5	-	XRD, RS (MEW)	[247]
$P\bar{4}2_1c$	β-Bi_2O_3	2	-	12	XRD, RS, DFT (MEW)	[243]

2.5. Mixed-Valence Sesquioxides

As mentioned in the introduction, there are A_2O_3 compounds where the A has two different valences, which constitute the subfamily MV-SOs. MV-SOs are highly interesting because they feature cations with different valences and consequently can be differently coordinated, thus resulting in a distortion in the structures of normal SOs. Examples of this kind of SOs are Sn_2O_3 and Pb_2O_3, where Sn and Pb cations show both 2+ and 4+ valences. While Pb_2O_3 has been known for almost a century [259] and crystallizes in the monoclinic s.g. $P2_1/a$ [260], Sn_2O_3 has just recently been predicted [261] and experimentally found to crystallize in the triclinic s.g. $P\bar{1}$ [262,263]. No HP studies on these two interesting but complex compounds have been reported to our knowledge.

3. Conclusions and Future Prospects

A great deal of work has been done on sesquioxides under compression and many pressure-induced phase transitions have been elucidated. In particular, the pressure-induced phase transitions of rare-earth sesquioxides and group-13 sesquioxides are quite well known, except for Tl_2O_3. The knowledge of pressure-induced phase transitions in transition-metal sesquioxides are not so well known, and those of group-15 sesquioxides have been recently studied, but still require more work. Finally, pressure-induced phase transitions in mixed-valence sesquioxides are completely unknown. It must be stressed that most of the high-pressure work done on sesquioxides corresponds to cubic, tetragonal, hexagonal, rhombohedral, and orthorhombic phases, while most of the high-pressure work still to be done on sesquioxides corresponds to complex monoclinic and triclinic phases. The study of these complex phases was rather difficult in the past, and is a challenge that must be accomplished in the 21st century with current and future experimental and theoretical techniques.

It must be noticed that the crystalline structures of the different subfamilies of sesquioxides and their pressure-induced phase transitions have some features in common. The archetypic structure of rare-earth sesquioxides is the C-type structure, which is isostructural to the bixbyite structure of several transition metal sesquioxides (Mn_2O_3) and group-13 sesquioxides (In_2O_3 and Tl_2O_3). On the other hand, the archetypic structure of group-13 and transition-metal sesquioxides is the corundum structure (Al_2O_3). In this context, it is remarkable that the pressure-induced transitions of C-type rare-earth sesquioxides, including Sc_2O_3 and Y_2O_3, are markedly different to those of C-type group-13 and transition-metal sesquioxides. In fact, these last compounds seem to have pressure-induced transitions

that are closer to those of corundum-type structures of group-13 and transition-metal sesquioxides. On the other hand, the crystalline structures and pressure-induced phase transitions of group-15 sesquioxides are completely different to those of other sesquioxides, due to the stereochemically active lone electron pair of group-15 cations, which lead to more open-framework structures than those present in other subfamilies. Consequently, we can speculate that a similar behavior is expected to be observed in future experiments of mixed-valence sesquioxides under compression, since this subfamily is also characterized by having some cations with lone electron pairs.

Finally, it should be mentioned that we are not aware of studies of negative pressures in sesquioxides. In principle, it is possible to reach absolute negative pressures (of the order of a few GPa) [264] where novel structures might appear [265]. In fact, negative pressures have been found in several solids, such $CaWO_4$ nanocrystals [266] and ice polymorphs [267]. Therefore, the application of negative pressures to materials is a route that can also be explored in sesquioxides, since it would lead to the expansion of the crystalline lattice, leading to the possible instability of the stable phase at room conditions in certain compounds, thus opening a new avenue to obtain novel and exotic metastable phases.

Author Contributions: F.J.M. contributed to the conceptualization and writing of the introduction, Sections 2.1 and 2.5 and conclusions; A.L.J.P. contributed to the writing of Section 2.2; J.I. contributed to the writing of Section 2.3 and J.A.S.T. contributed to the writing of Section 2.4 and the revision of the manuscript.

Funding: This research was funded by Spanish Ministerio de Ciencia, Innovación y Universidades under grants MAT2016-75586-C4-1/2/3-P, FIS2017-83295-P, PGC2018-094417-B-100, and RED2018-102612-T (MALTA-Consolider-Team network) and by Generalitat Valenciana under grant PROMETEO/2018/123 (EFIMAT). J. A. S. also acknowledges Ramón y Cajal Fellowship for financial support (RYC-2015-17482).

Conflicts of Interest: The authors declare no conflict of interest. The funders had no role in the design of the study; in the collection, analyses, or interpretation of data; in the writing of the manuscript, or in the decision to publish the results.

References

1. Liu, L.-G.; Bassett, W.A. *Elements, Oxides, Silicates, High-Pressure Phases with Implications for the Earth's Interior*; Oxford Monographs on Geology and Geophysics; Oxford University Press: Oxford, UK, 1986; Volume 4.
2. Adachi, G.-Y.; Imanaka, N. The Binary Rare Earth Oxides. *Chem. Rev.* **1998**, *98*, 1479–1514. [CrossRef] [PubMed]
3. Smyth, J.R.; Jacobsen, S.D.; Hazen, R.M. Comparative Crystal Chemistry of Dense Oxide Minerals. In *Reviews in Mineralogy and Geochemistry*; Mineralogical Society of America: Chantilly, VA, USA, 2000; Volume 41.
4. Zinkevich, M. Thermodynamics of rare earth sesquioxides. *Prog. Mat. Sci.* **2007**, *52*, 597–647. [CrossRef]
5. Manjón, F.J.; Errandonea, D. Pressure-induced structural phase transitions in materials science. *Phys. Stat. Sol. B* **2009**, *246*, 9–31. [CrossRef]
6. Foex, M.; Traverse, J.P. Remarques sur les transformations cristallines presentees a haute temperature par les sesquioxydes de terres rares. *Rev. Int. Hautes Temp. Refract.* **1966**, *3*, 429–453.
7. Hoekstra, H.R.; Gingerich, K.A. High-Pressure B-Type Polymorphs of Some Rare-Earth Sesquioxides. *Science* **1964**, *14*, 1163–1164. [CrossRef]
8. Sawyer, J.O.; Hyde, B.G.; Eyring, L. Pressure and Polymorphism in the Rare Earth Sesquioxides. *Inorg. Chem.* **1965**, *4*, 426–427. [CrossRef]
9. Vegas, A.; Isea, R. Distribution of the M-M Distances in the Rare Earth Oxides. *Acta Cryst. B* **1998**, *54*, 732–740. [CrossRef]
10. Vegas, A. *Structural Models of Inorganic Crystals*; Editorial Universitat Politècnica de Valencia: Valencia, Spain, 2018.
11. McClure, J.P. High Pressure Phase Transistions in the Lanthanide Sesquioxides. Ph.D. Thesis, University of Nevada, Las Vegas, NV, USA, 2009.
12. Jiang, S.; Liu, J.; Lin, C.L.; Bai, L.G.; Xiao, W.S.; Zhang, Y.F.; Zhang, D.C.; Li, X.D.; Li, Y.C.; Tang, L.Y. Pressure-induced phase transition in cubic Lu_2O_3. *J. Appl. Phys.* **2010**, *108*, 083541. [CrossRef]
13. Lin, C.-M.; Wu, K.-T.; Hung, T.-L.; Sheu, H.-S.; Tsai, M.-H.; Lee, J.-F.; Lee, J.-J. Phase transitions in Lu_2O_3 under high pressure. *Solid State Commun.* **2010**, *150*, 1564–1569. [CrossRef]

14. Yusa, H.; Kikegawa, T. *Photon Factory Activity Report #28 Part B 223*; Kishimoto, S., Ed.; High Energy Accelerator Research Organization (KEK): Ibaraki, Japan, 2010.
15. Meyer, C.; Sanchez, J.P.; Thomasson, J.; Itié, J.P. Mossbauer and energy-dispersive x-ray-diffraction studies of the pressure-induced crystallographic phase transition in C-type Yb_2O_3. *Phys. Rev. B* **1995**, *51*, 12187–12193. [CrossRef]
16. Yusa, H.; Kikegawa, T.; Tsuchiya, T. *Photon Factory Activity Report #27 Part B 195*; Iwano, K., Ed.; High Energy Accelerator Research Organization (KEK): Ibaraki, Japan, 2009.
17. Lonappan, D. High Pressure Phase Transformation Studies on Rare Earth Sesquioxides. Ph.D. Thesis, Indira Gandhi Centre for Atomic Research, Tamil Nadu, India, 2012.
18. Pandey, S.D.; Samanta, K.; Singh, J.; Sharma, N.D.; Bandyopadhyay, A.K. Anharmonic behavior and structural phase transition in Yb_2O_3. *AIP Adv.* **2013**, *3*, 122123. [CrossRef]
19. Sahu, P.C.; Lonappan, D.; Chandra Shekar, N.V. High Pressure Structural Studies on Rare-Earth Sesquioxides. *J. Phys. Conf. Ser.* **2012**, *377*, 012015. [CrossRef]
20. Irshad, K.A.; Anees, P.; Sahoo, S.; Sanjay Kumar, N.R.; Srihari, V.; Kalavathi, S.; Chandra Shekar, N.V. Pressure induced structural phase transition in rare earth sesquioxide Tm_2O_3: Experiment and *ab initio* calculations. *J. Appl. Phys.* **2018**, *124*, 155901. [CrossRef]
21. Yan, D.; Wu, P.; Zhang, S.P.; Liang, L.; Yang, F.; Pei, Y.L.; Chen, S. Assignments of the Raman modes of monoclinic erbium oxide. *J. Appl. Phys.* **2013**, *114*, 193502. [CrossRef]
22. Ren, X.T.; Yan, X.Z.; Yu, Z.H.; Li, W.T.; Wang, L. Photoluminescence and phase transition in Er_2O_3 under high pressure. *J. Alloy. Compd.* **2017**, *725*, 941–945. [CrossRef]
23. Lonappan, D.; Chandra Shekar, N.V.; Ravindran, T.R.; Sahu, P.C. High-pressure phase transition in Ho_2O_3. *Mater. Chem. Phys.* **2010**, *120*, 65–67. [CrossRef]
24. Jiang, S.; Liu, J.; Li, X.D.; Bai, L.G.; Xiao, W.S.; Zhang, Y.F.; Lin, C.L.; Li, Y.C.; Tang, L.Y. Phase transformation of Ho_2O_3 at high pressure. *J. Appl. Phys.* **2011**, *110*, 013526. [CrossRef]
25. Pandey, S.D.; Samanta, K.; Singh, J.; Sharma, N.D.; Bandyopadhyay, A.K. Raman scattering of rare earth sesquioxide Ho_2O_3: A pressure and temperature dependent study. *J. Appl. Phys.* **2014**, *116*, 133504. [CrossRef]
26. Yan, X.Z.; Ren, X.T.; He, D.W.; Chen, B.; Yang, W.G. Mechanical behaviors and phase transition of Ho_2O_3 nanocrystals under high pressure. *J. Appl. Phys.* **2014**, *116*, 033507. [CrossRef]
27. Sharma, N.D.; Singh, J.; Dogra, S.; Varandani, D.; Poswal, H.K.; Sharma, S.M.; Bandyopadhyay, A.K. Pressure-induced anomalous phase transformation in nano-crystalline dysprosium sesquioxide. *J. Raman Spectrosc.* **2011**, *42*, 438–444. [CrossRef]
28. Jiang, S.; Liu, J.; Lin, C.L.; Bai, L.G.; Zhang, Y.F.; Li, X.D.; Li, Y.C.; Tang, L.Y.; Wang, H. Structural transformations in cubic Dy_2O_3 at high pressures. *Solid State Commun.* **2013**, *169*, 37–41. [CrossRef]
29. Chen, H.Y.; He, C.Y.; Gao, C.X.; Ma, Y.M.; Zhang, J.H.; Wang, X.J.; Gao, S.Y.; Li, D.M.; Kan, S.H.; Zou, G.T. The structural transition of Gd_2O_3 nanoparticles induced by high pressure. *J. Phys. Condens. Matter* **2007**, *19*, 425229. [CrossRef]
30. Chen, H.Y.; He, C.Y.; Gao, C.X.; Ma, Y.M.; Zhang, J.H.; Gao, S.Y.; Lu, H.L.; Nie, Y.G.; Li, D.M.; Kan, S.H.; et al. Structural Transition of Gd_2O_3: Eu Induced by High Pressure. *Chin. Phys. Lett.* **2007**, *24*, 158–160. [CrossRef]
31. Zhang, F.X.; Lang, M.; Wang, J.W.; Becker, U.; Ewing, R.C. Structural phase transitions of cubic Gd_2O_3 at high pressures. *Phys. Rev. B* **2008**, *78*, 064114. [CrossRef]
32. Dilawar, N.; Varandani, D.; Mehrotra, S.; Poswal, H.K.; Sharma, S.M.; Bandyopadhyay, A.K. Anomalous high pressure behaviour in nanosized rare earth sesquioxides. *Nanotechnology* **2008**, *19*, 115703. [CrossRef] [PubMed]
33. Bai, L.G.; Liu, J.; Li, X.D.; Jiang, S.; Xiao, W.S.; Li, Y.C.; Tang, L.Y.; Zhang, Y.F.; Zhang, D.C. Pressure-induced phase transformations in cubic Gd_2O_3. *J. Appl. Phys.* **2009**, *106*, 073507. [CrossRef]
34. Zou, X.; Gong, C.; Liu, B.B.; Li, Q.J.; Li, Z.P.; Liu, B.; Liu, R.; Liu, J.; Chen, Z.Q.; Zou, B.; et al. X-ray diffraction of cubic Gd_2O_3/Er under high pressure. *Phys. Stat. Sol. B* **2011**, *248*, 1123–1127. [CrossRef]
35. Zhang, C.C.; Zhang, Z.M.; Dai, R.C.; Wang, Z.P.; Ding, Z.J. High Pressure Luminescence and Raman Studies on the Phase Transition of Gd_2O_3:Eu^{3+} Nanorods. *J. Nanosci. Nanotechnol.* **2011**, *11*, 9887–9891. [CrossRef] [PubMed]

36. Yang, X.; Li, Q.J.; Liu, Z.D.; Bai, X.; Song, H.W.; Yao, M.G.; Liu, B.; Liu, R.; Gong, C.; Lu, S.C.; et al. Pressure-Induced Amorphization in Gd_2O_3/Er^{3+} Nanorods. *J. Phys. Chem. C* **2013**, *117*, 8503–8508. [CrossRef]
37. Chen, G.; Haire, R.G.; Peterson, J.R. Effect of pressure on cubic (C-type) Eu_2O_3 studied via Eu^{3+} luminescence. *High Press. Res.* **1991**, *6*, 371–377. [CrossRef]
38. Chen, G.; Stump, N.A.; Haire, R.G.; Peterson, J.R. Study of the phase behavior of Eu_2O_3 under pressure via luminescence of Eu^{3+}. *J. Alloy. Compd.* **1992**, *181*, 503–509. [CrossRef]
39. Dilawar, N.; Varandani, D.; Pandey, V.P.; Kumar, M.; Shivaprasad, S.M.; Sharma, P.K.; Bandyopadhyay, A.K. Structural Transition in Nanostructured Eu_2O_3 Under High Pressures. *J. Nanosci. Nanotechnol.* **2006**, *6*, 105–113. [PubMed]
40. Jiang, S.; Bai, L.G.; Liu, J.; Xiao, W.S.; Li, X.D.; Li, Y.C.; Tang, L.Y.; Zhang, Y.F.; Zhang, D.C.; Zheng, L.R. The Phase Transition of Eu_2O_3 under High Pressures. *Chin. Phys. Lett.* **2006**, *26*, 076101.
41. Irshad, K.A.; Chandra Shekar, N.V.; Srihari, V.; Pandey, K.K.; Kalavathi, S. High pressure structural phase transitions in Ho: Eu_2O_3. *J. Alloy. Compd.* **2017**, *725*, 911–915. [CrossRef]
42. Irshad, K.A.; Chandra Shekar, N.V. Anomalous lattice compressibility of hexagonal Eu_2O_3. *Mat. Chem. Phys.* **2017**, *195*, 88–93. [CrossRef]
43. Yu, Z.H.; Wang, Q.L.; Ma, Y.Z.; Wang, L. X-ray diffraction and spectroscopy study of nano-Eu_2O_3 structural transformation under high pressure. *J. Alloy. Compd.* **2017**, *701*, 542–548. [CrossRef]
44. Guo, Q.X.; Zhao, Y.S.; Jiang, C.; Mao, W.L.; Wang, Z.W. Phase transformation in Sm_2O_3 at high pressure: In situ synchrotron X-ray diffraction study and ab initio DFT calculation. *Solid State Commun.* **2008**, *145*, 250–254. [CrossRef]
45. Jiang, S.; Liu, J.; Lin, C.L.; Li, X.D.; Li, Y.C. High-pressure x-ray diffraction and Raman spectroscopy of phase transitions in Sm_2O_3. *J. Appl. Phys.* **2013**, *113*, 113502. [CrossRef]
46. Liu, D.; Lei, W.W.; Li, Y.W.; Ma, Y.M.; Hao, J.; Chen, X.H.; Jin, Y.X.; Liu, D.; Yu, S.D.; Cui, Q.L.; et al. High-Pressure Structural Transitions of Sc_2O_3 by X-ray Diffraction, Raman Spectra, and Ab Initio Calculations. *Inorg. Chem.* **2009**, *48*, 8251–8256. [CrossRef]
47. Yusa, H.; Tsuchiya, T.; Sata, N.; Ohishi, Y. High-Pressure Phase Transition to the Gd_2S_3 Structure in Sc_2O_3: A New Trend in Dense Structures in Sesquioxides. *Inorg. Chem.* **2009**, *48*, 7537–7543. [CrossRef]
48. Ovsyannikov, S.V.; Bykova, E.; Bykov, M.; Wenz, M.D.; Pakhomova, A.S.; Glazyrin, K.; Liermann, H.-P.; Dubrovinsky, L. Structural and vibrational properties of single crystals of Scandia, Sc_2O_3 under high pressure. *J. Appl. Phys.* **2015**, *118*, 165901. [CrossRef]
49. Husson, E.; Proust, C.; Gillet, P.; Itié, J.P. Phase transitions in yttrium oxide at high pressure studied by Raman spectroscopy. *Mater. Res. Bull.* **1999**, *34*, 2085–2092. [CrossRef]
50. Bai, X.; Song, H.W.; Liu, B.B.; Hou, Y.Y.; Pan, G.H.; Ren, X.G. Effects of High Pressure on the Luminescence Properties of Nanocrystalline and Bulk Y_2O_3:Eu^{3+}. *J. Nanosci. Nanotechnol.* **2008**, *8*, 1404–1409. [CrossRef] [PubMed]
51. Jovanic, B.R.; Dramicanin, M.; Viana, B.; Panic, B.; Radenkovic, B. High-pressure optical studies of Y_2O_3:Eu^{3+} nanoparticles. *Radiat. Eff. Defects Solids* **2008**, *163*, 925–931. [CrossRef]
52. Wang, L.; Pan, Y.X.; Ding, Y.; Yang, W.G.; Mao, W.L.; Sinogeikin, S.V.; Meng, Y.; Shen, G.Y.; Mao, H.-K. High-pressure induced phase transitions of Y_2O_3 and Y_2O_3:Eu^{3+}. *Appl. Phys. Lett.* **2009**, *94*, 061921. [CrossRef]
53. Wang, L.; Yang, W.; Ding, Y.; Ren, Y.; Xiao, S.G.; Liu, B.B.; Sinogeikin, S.V.; Meng, Y.; Gosztola, D.J.; Shen, G.Y.; et al. Size-Dependent Amorphization of Nanoscale Y_2O_3 at High Pressure. *Phys. Rev. Lett.* **2010**, *105*, 095701. [CrossRef]
54. Halevy, I.; Carmon, R.; Winterrose, M.L.; Yeheskel, O.; Tiferet, E.; Ghose, S. Pressure-induced structural phase transitions in Y_2O_3 sesquioxide. *J. Phys. Conf. Ser.* **2010**, *215*, 012003. [CrossRef]
55. Dai, R.C.; Zhang, Z.M.; Zhang, C.C.; Ding, Z.J. Photoluminescence and Raman Studies of Y_2O_3:Eu^{3+} Nanotubes Under High Pressure. *J. Nanosci. Nanotechnol.* **2010**, *10*, 7629–7633. [CrossRef]
56. Dai, R.C.; Wang, Z.P.; Zhang, Z.M.; Ding, Z.J. Photoluminescence study of SiO_2 coated Eu^{3+}:Y_2O_3 core-shells under high pressure. *J. Rare Earth* **2010**, *28*, 241–245. [CrossRef]
57. Yusa, H.; Tsuchiya, T.; Sata, N.; Ohishi, Y. Dense Yttria Phase Eclipsing the A-Type Sesquioxide Structure: High-Pressure Experiments and ab initio Calculations. *Inorg. Chem.* **2010**, *49*, 4478–4485. [CrossRef]

58. Bose, P.P.; Gupta, M.K.; Mittal, R.; Rols, S.; Achary, S.N.; Tyagi, A.K.; Chaplot, S.L. High Pressure Phase Transitions in Yttria, Y_2O_3. *J. Phys. Conf. Ser.* **2012**, *377*, 012036. [CrossRef]
59. Srivastava, A.M.; Renero-Lecuna, C.; Santamaría-Pérez, D.; Rodríguez, F.; Valiente, R. Pressure-induced Pr^{3+} $^3P_0$ luminescence in cubic Y_2O_3. *J. Lumin.* **2014**, *146*, 27–32. [CrossRef]
60. Jiang, S.; Liu, J.; Li, X.-D.; Li, Y.-C.; He, S.-M.; Zhang, J.-C. High-Pressure Phase Transitions of Cubic Y_2O_3 under High Pressures by In-situ Synchrotron X-Ray Diffraction. *Chin. Phys. Lett.* **2019**, *36*, 046103. [CrossRef]
61. Ibáñez, J.; Sans, J.A.; Cuenca-Gotor, V.; Oliva, R.; Blázquez, O.; Gomis, O.; Rodríguez-Hernández, P.; Muñoz, A.; Rodríguez-Mendoza, U.R.; Velázquez, M.; et al. Experimental and theoretical study of Tb_2O_3 under compression. Manuscript in preparation for 2020.
62. Zhang, Q.; Wu, X.; Qin, S. Pressure-induced phase transition of B-type Y_2O_3. *Chin. Phys. B* **2017**, *26*, 090703. [CrossRef]
63. Chen, G.; Peterson, J.R.; Brister, K.E. An Energy-Dispersive X-Ray Diffraction Study of Monoclinic Eu_2O_3 under Pressure. *J. Solid State Chem.* **1994**, *111*, 437–439. [CrossRef]
64. Atou, T.; Kusaba, K.; Tsuchida, Y.; Utsumi, W.; Yagi, T.; Syono, Y. Reversible B-type- A-type transition of Sm_2O_3 under high pressure. *Mater. Res. Bull.* **1989**, *24*, 1171–1176. [CrossRef]
65. Hongo, T.; Kondo, K.; Nakamura, K.G.; Atou, T. High pressure Raman spectroscopic study of structural phase transition in samarium oxide. *J. Mater. Sci.* **2007**, *42*, 2582–2585. [CrossRef]
66. Guo, Q.X.; Zhao, Y.S.; Jiang, C.; Mao, W.L.; Wang, Z.W.; Zhang, J.Z.; Wang, Y.J. Pressure-Induced Cubic to Monoclinic Phase Transformation in Erbium Sesquioxide Er_2O_3. *Inorg. Chem.* **2007**, *46*, 6164–6169. [CrossRef]
67. Pandey, K.K.; Garg, N.; Mishra, A.K.; Sharma, S.M. High pressure phase transition in Nd_2O_3. *J. Phys. Conf. Ser.* **2012**, *377*, 012006. [CrossRef]
68. Jiang, S.; Liu, J.; Bai, L.G.; Li, X.D.; Li, Y.C.; He, S.M.; Yan, S.; Liang, D.X. Anomalous compression behaviour in Nd_2O_3 studied by x-ray diffraction and Raman spectroscopy. *AIP Adv.* **2018**, *8*, 025019. [CrossRef]
69. Lipp, M.J.; Jeffries, J.R.; Cynn, H.; Park Klepeis, J.H.; Evans, W.J.; Mortensen, D.R.; Seidler, G.T.; Xiao, Y.; Chow, P. Comparison of the high-pressure behavior of the cerium oxides Ce_2O_3 and CeO_2. *Phys. Rev. B* **2016**, *93*, 064106. [CrossRef]
70. Hirosaki, N.; Ogata, S.; Kocer, C. Ab initio calculation of the crystal structure of the lanthanide Ln_2O_3 sesquioxides. *J. Alloy. Compd.* **2003**, *351*, 31–34. [CrossRef]
71. Marsella, L.; Fiorentini, V. Structure and stability of rare-earth and transition-metal oxides. *Phys. Rev. B* **2004**, *69*, 172103. [CrossRef]
72. Petit, L.; Svane, A.; Szotec, Z.; Temmerman, W.M. First-principles study of rare-earth oxides. *Phys. Rev. B* **2005**, *72*, 205118. [CrossRef]
73. Wu, B.; Zinkevich, M.; Chong, W.A.N.G.; Aldinger, F. Ab initio energetic study of oxide ceramics with rare-earth elements. *Rare Met.* **2006**, *25*, 549–555. [CrossRef]
74. Singh, N.; Saini, S.M.; Nautiyal, T.; Auluck, S. Electronic structure and optical properties of rare earth sesquioxides (R_2O_3, R = La, Pr, and Nd). *J. Appl. Phys.* **2006**, *100*, 083525. [CrossRef]
75. Mikami, M.; Nakamura, S. Electronic structure of rare-earth sesquioxides and oxysulfides. *J. Alloy. Compd.* **2006**, *408–412*, 687–692. [CrossRef]
76. Wu, B.; Zinkevich, M.; Aldinger, F.; Wen, D.Z.; Chen, L. Ab initio study on structure and phase transition of A- and B-type rare-earth sesquioxides Ln_2O_3 (Ln = La–Lu, Y, and Sc) based on density function theory. *J. Solid State Chem.* **2007**, *180*, 3280–3287. [CrossRef]
77. Rahm, M.; Skorodumova, N.V. Phase stability of the rare-earth sesquioxides under pressure. *Phys. Rev. B* **2009**, *80*, 104105. [CrossRef]
78. Jiang, H.; Gomez-Abal, R.I.; Rinke, P.; Scheffler, M. Localized and Itinerant States in Lanthanide Oxides United by GW@LDA+U. *Phys. Rev. Lett.* **2009**, *102*, 126403. [CrossRef] [PubMed]
79. Gillen, R.; Clark, S.J.; Robertson, J. Nature of the electronic band gap in lanthanide oxides. *Phys. Rev. B* **2013**, *87*, 125116. [CrossRef]
80. Richard, D.; Muñoz, E.L.; Rentería, M.; Errico, L.A.; Svane, A.; Christensen, N.E. Ab initio LSDA and LSDA+U study of pure and Cd-doped cubic lanthanide sesquioxides. *Phys. Rev. B* **2013**, *88*, 165206. [CrossRef]
81. Richard, D.; Errico, L.A.; Rentería, M. Structural properties and the pressure-induced C → A phase transition of lanthanide sesquioxides from DFT and DFT+U calculations. *J. Alloy. Compd.* **2016**, *664*, 580–589. [CrossRef]

82. Ogawa, T.; Otani, N.; Yokoi, T.; Fisher, C.A.J.; Kuwabara, A.; Moriwake, H.; Yoshiya, M.; Kitaoka, S.; Takata, M. Density functional study of phase stabilities and Raman spectra of Yb_2O_3, Yb_2SiO_5 and $Yb_2Si_2O_7$ under pressure. *Phys. Chem. Chem. Phys.* **2018**, *20*, 16518–16527. [CrossRef]
83. Pathak, A.K.; Vazhappily, T. Ab Initio Study on Structure, Elastic, and Mechanical Properties of Lanthanide Sesquioxides. *Phys. Stat. Sol. B* **2018**, *255*, 1700668. [CrossRef]
84. Catlow, C.R.A.; Guo, Z.X.; Miskufova, M.; Shevlin, S.A.; Smith, A.G.H.; Sokol, A.A.; Walsh, A.; Wilson, D.J.; Woodley, S.M. Advances in computational studies of energy materials. *Philos. Trans. R. Soc. A Math. Phys. Eng. Sci.* **2010**, *368*, 3379–3456. [CrossRef]
85. Caracas, R.; Cohen, R.E. Prediction of a new phase transition in Al_2O_3 at high pressures. *Geophys. Res. Lett.* **2005**, *32*, 1–4. [CrossRef]
86. Funamori, N. High-Pressure Transformation of Al_2O_3. *Science* **1997**, *278*, 1109–1111. [CrossRef]
87. Cynn, H.; Isaak, D.G.; Cohen, R.E.; Nicol, M.F.; Anderson, O.L. A high-pressure phase transition of corundum predicted by the potential induced breathing model. *Am. Mineral.* **1990**, *75*, 439–442.
88. Jephcoat, A.P.; Hemley, R.J.; Mao, H.K. X-ray diffraction of ruby (Al_2O_3:Cr^{3+}) to 175 GPa. *Phys. B C* **1988**, *150*, 115–121. [CrossRef]
89. Dewaele, A.; Torrent, M. Equation of state of α-Al_2O_3. *Phys. Rev. B* **2013**, *88*, 064107. [CrossRef]
90. Costa, T.M.H.; Gallas, M.R.; Benvenutti, E.V.; da Jornada, J.A.H. Study of Nanocrystalline γ-Al_2O_3 Produced by High-Pressure Compaction. *J. Phys. Chem. B* **1999**, *103*, 4278–4284. [CrossRef]
91. Hart, H.V.; Drickamer, H.G. Effect of high pressure on the lattice parameters of Al_2O_3. *J. Chem. Phys.* **1965**, *43*, 2265–2266. [CrossRef]
92. Marton, F.C.; Cohen, R.E. Prediction of a high-pressure phase transition in Al_2O_3. *Am. Miner.* **1994**, *79*, 789–792.
93. Mashimo, T.; Tsumoto, K.; Nakamura, K.; Noguchi, Y.; Fukuoka, K.; Syono, Y. High-pressure phase transformation of corundum (α-Al_2O_3) observed under shock compression. *Geophys. Res. Lett.* **2000**, *27*, 2021–2024. [CrossRef]
94. Ono, S.; Oganov, A.R.; Koyama, T.; Shimizu, H. Stability and compressibility of the high-pressure phases of Al_2O_3 up to 200 GPa: Implications for the electrical conductivity of the base of the lower mantle. *Earth Planet. Sci. Lett.* **2006**, *246*, 326–335. [CrossRef]
95. Zhao, J.; Hearne, G.R.; Maaza, M.; Laher-Lacour, F.; Witcomb, M.J.; Le Bihan, T.; Mezouar, M. Compressibility of nanostructured alumina phases determined from synchrotron x-ray diffraction studies at high pressure. *J. Appl. Phys.* **2001**, *90*, 3280–3285. [CrossRef]
96. Thomson, K.T.; Wentzcovitch, R.M.; Bukowinski, M.S.T. Polymorphs of alumina predicted by first principles: Putting pressure on the ruby pressure scale. *Science* **1996**, *274*, 1880–1882. [CrossRef]
97. Lin, J.F.; Degtyareva, O.; Prewitt, C.T.; Dera, P.; Sata, N.; Gregoryanz, E.; Mao, H.K.; Hemley, R.J. Crystal structure of a high-pressure/high-temperature phase of alumina by in situ X-ray diffraction. *Nat. Mater.* **2004**, *3*, 389–393. [CrossRef]
98. Jahn, S.; Madden, P.A.; Wilson, M. Dynamic simulation of pressure-driven phase transformations in crystalline Al_2O_3. *Phys. Rev. B* **2004**, *69*, 020106. [CrossRef]
99. Tsuchiya, J.; Tsuchiya, T.; Wentzcovitch, R.M. Transition from the Rh_2O_3(II)-to-$CaIrO_3$ structure and the high-pressure-temperature phase diagram of alumina. *Phys. Rev. B* **2005**, *72*, 020103. [CrossRef]
100. Garcia-Domene, B.; Ortiz, H.M.; Gomis, O.; Sans, J.A.; Manjón, F.J.; Muñoz, A.; Rodríguez-Hernández, P.; Achary, S.N.; Errandonea, D.; Martínez-García, D.; et al. High-pressure lattice dynamical study of bulk and nanocrystalline In_2O_3. *J. Appl. Phys.* **2012**, *112*, 123511. [CrossRef]
101. García-Domene, B.; Sans, J.A.; Gomis, O.; Manjón, F.J.; Ortiz, H.M.; Errandonea, D.; Santamaría-Pérez, D.; Martínez-García, D.; Vilaplana, R.; Pereira, A.L.J.; et al. Pbca-type In_2O_3: The high-pressure post-corundum phase at room temperature. *J. Phys. Chem. C* **2014**, *118*, 20545–20552. [CrossRef]
102. Gurlo, A. Structural stability of high-pressure polymorphs in In_2O_3 nanocrystals: Evidence of stress-induced transition? *Angew. Chem. Int. Ed.* **2010**, *49*, 5610–5612. [CrossRef]
103. Liu, D.; Lei, W.W.; Zou, B.; Yu, S.D.; Hao, J.; Wang, K.; Liu, B.B.; Cui, Q.L.; Zou, G.T. High-pressure x-ray diffraction and Raman spectra study of indium oxide. *J. Appl. Phys.* **2008**, *104*, 083506. [CrossRef]
104. Qi, J.; Liu, J.F.; He, Y.; Chen, W.; Wang, C. Compression behavior and phase transition of cubic In_2O_3 nanocrystals. *J. Appl. Phys.* **2011**, *109*, 063520. [CrossRef]

105. Tang, S.; Li, Y.; Zhang, J.; Zhu, H.; Dong, Y.; Zhu, P.; Cui, Q. Effects of microstructures on the compression behavior and phase transition routine of In_2O_3 nanocubes under high pressures. *RSC Adv.* **2015**, *5*, 85105–85110. [CrossRef]
106. Yusa, H.; Tsuchiya, T.; Sata, N.; Ohishi, Y. Rh_2O_3(II)-type structures in Ga_2O_3 and In_2O_3 under high pressure: Experiment and theory. *Phys. Rev. B* **2008**, *77*, 064107. [CrossRef]
107. Yusa, H.; Tsuchiya, T.; Tsuchiya, J.; Sata, N.; Ohishi, Y. α-Gd_2S_3-type structure in In_2O_3: Experiments and theoretical confirmation of a high-pressure polymorph in sesquioxide. *Phys. Rev. B* **2008**, *78*, 092107. [CrossRef]
108. García-Domene, B.; Sans, J.A.; Manjón, F.J.; Ovsyannikov, S.V.; Dubrovinsky, L.S.; Martinez-Garcia, D.; Gomis, O.; Errandonea, D.; Moutaabbid, H.; Le Godec, Y.; et al. Synthesis and High-Pressure Study of Corundum-Type In_2O_3. *J. Phys. Chem. C* **2015**, *119*, 29076–29087. [CrossRef]
109. Sans, J.A.; Vilaplana, R.; Errandonea, D.; Cuenca-Gotor, V.P.; García-Domene, B.; Popescu, C.; Manjón, F.J.; Singhal, A.; Achary, S.N.; Martinez-Garcia, D.; et al. Structural and vibrational properties of corundum-type In_2O_3 nanocrystals under compression. *Nanotechnology* **2017**, *28*, 205701. [CrossRef] [PubMed]
110. Lipinska-Kalita, K.E.; Kalita, P.E.; Hemmers, O.A.; Hartmann, T. Equation of state of gallium oxide to 70 GPa: Comparison of quasihydrostatic and nonhydrostatic compression. *Phys. Rev. B* **2008**, *77*, 094123. [CrossRef]
111. Lipinska-Kalita, K.E.; Chen, B.; Kruger, M.B.; Ohki, Y.; Murowchick, J.; Gogol, E.P. High-pressure x-ray diffraction studies of the nanostructured transparent vitroceramic medium K_2O-SiO_2-Ga_2O_3. *Phys. Rev. B* **2003**, *68*, 035209. [CrossRef]
112. Luan, S.; Dong, L.; Jia, R. Analysis of the structural, anisotropic elastic and electronic properties of β-Ga_2O_3 with various pressures. *J. Cryst. Growth* **2019**, *505*, 74–81. [CrossRef]
113. Machon, D.; McMillan, P.F.; Xu, B.; Dong, J. High-pressure study of the β-to-α transition in Ga_2O_3. *Phys. Rev. B* **2006**, *73*, 094125. [CrossRef]
114. Wang, H.; He, Y.; Chen, W.; Zeng, Y.W.; Stahl, K.; Kikegawa, T.; Jiang, J.Z. High-pressure behavior of β-Ga_2O_3 nanocrystals. *J. Appl. Phys.* **2010**, *107*, 033520. [CrossRef]
115. Claussen, W.F.; Mackenzie, J.D. Crystallization of B_2O_3 at High Pressures. *J. Am. Chem. Soc.* **1959**, *81*, 1007. [CrossRef]
116. Prewitt, C.T.; Shannon, R.D. Crystal structure of a high-pressure form of B_2O_3. *Acta Crystallogr. Sect. B Struct. Crystallogr. Cryst. Chem.* **1968**, *24*, 869–874. [CrossRef]
117. Brazhkin, V.V.; Katayama, Y.; Inamura, Y.; Kondrin, M.V.; Lyapin, A.G.; Popova, S.V.; Voloshin, R.N. Structural transformations in liquid, crystalline, and glassy B_2O_3 under high pressure. *JETP Lett.* **2003**, *78*, 393–397. [CrossRef]
118. Nicholas, J.; Sinogeikin, S.; Kieffer, J.; Bass, J. Spectroscopic evidence of polymorphism in vitreous B_2O_3. *Phys. Rev. Lett.* **2004**, *92*, 3–6. [CrossRef] [PubMed]
119. Lee, S.K.; Mibe, K.; Fei, Y.; Cody, G.D.; Mysen, B.O. Structure of B_2O_3 glass at high pressure: A 11B solid-state NMR study. *Phys. Rev. Lett.* **2005**, *94*, 27–30. [CrossRef] [PubMed]
120. Kulikova, L.F.; Dyuzheva, T.I.; Nikolaev, N.A.; Brazhkin, V.V. Single-crystal growth of the high-pressure phase B_2O_3 II. *Crystallogr. Rep.* **2012**, *57*, 332–335. [CrossRef]
121. Burianek, M.; Birkenstock, J.; Mair, P.; Kahlenberg, V.; Medenbach, O.; Shannon, R.D.; Fischer, R.X. High-pressure synthesis, long-term stability of single crystals of diboron trioxide, B_2O_3, and an empirical electronic polarizability of [3]B^{3+}. *Phys. Chem. Miner.* **2016**, *43*, 527–534. [CrossRef]
122. Gomis, O.; Santamaría-Pérez, D.; Ruiz-Fuertes, J.; Sans, J.A.; Vilaplana, R.; Ortiz, H.M.; García-Domene, B.; Manjón, F.J.; Errandonea, D.; Rodríguez-Hernández, P.; et al. High-pressure structural and elastic properties of Tl_2O_3. *J. Appl. Phys.* **2014**, *116*, 133521. [CrossRef]
123. Weir, S.T.; Mitchell, A.C.; Nellis, W.J. Electrical resistivity of single-crystal Al_2O_3 shock-compressed in the pressure range 91-220 GPa (0.91-2.20 Mbar). *J. Appl. Phys.* **1996**, *80*, 1522–1525. [CrossRef]
124. Syassen, K. Ruby under pressure. *High Press. Res.* **2008**, *28*, 75–126. [CrossRef]
125. Smyth, J.R.; Jacobsen, S.D.; Hazen, R.M. Comparative Crystal Chemistry of Dense Oxide Minerals. *Rev. Miner. Geochem.* **2000**, *41*, 157–186. [CrossRef]
126. Song, H.I.; Kim, E.S.; Yoon, K.H. Phase transformation and characteristics of beta-alumina. *Phys. B C* **1988**, *150*, 148–159. [CrossRef]

127. Engürlu, S.; Taslicukur Öztürk, Z.; Kuskonmaz, N. Investigation of the Production of β-Al_2O_3 Solid Electrolyte from Seydişehir α-Al_2O_3. *Süleyman Demirel Üniversitesi Fen Bilimleri Enstitüsü Derg.* **2017**, *21*, 816. [CrossRef]
128. Duan, W.; Wentzcovitch, R.M.; Thomson, K.T. First-principles study of high-pressure alumina polymorphs. *Phys. Rev. B* **1998**, *57*, 10363–10369. [CrossRef]
129. Oganov, A.R.; Ono, S. The high-pressure phase of alumina and implications for Earth's D" layer. *Proc. Natl. Acad. Sci. USA* **2005**, *102*, 10828–10831. [CrossRef]
130. Hama, J.; Suito, K. The evidence for the occurrence of two successive transitions in Al_2O_3 from the analysis of Hugoniot data. *High Temp. High Press.* **2002**, *34*, 323–334. [CrossRef]
131. Ono, S.; Kikegawa, T.; Ohishi, Y. High-pressure phase transition of hematite, Fe_2O_3. *J. Phys. Chem. Solids* **2004**, *65*, 1527–1530. [CrossRef]
132. Oganov, A.R.; Ono, S. Theoretical and experimental evidence for a post-perovskite phase of $MgSiO_3$ in Earth's D" layer. *Nature* **2004**, *430*, 445–448. [CrossRef]
133. Vaidya, S.N. High-pressure high-temperature transitions in nanocrystalline γ Al_2O_3, γ Fe_2O_3 and TiO_2. *Bull. Mater. Sci.* **1999**, *22*, 287–293. [CrossRef]
134. Mishra, R.S.; Lesher, C.E.; Mukherjee, A.K. High-Pressure Sintering of Nanocrystalline gamma Al_2O_3. *J. Am. Ceram. Soc.* **1996**, *79*, 2989–2992. [CrossRef]
135. Vaidya, S.N.; Karunakaran, C.; Achary, S.N.; Tyagi, A.K. New polymorphs of alumina. *High Press. Res.* **1999**, *16*, 147–160. [CrossRef]
136. Vaidya, S.N.; Karunakaran, C.; Achary, S.N.; Tyagi, A.K. New polymorphs of alumina: Part II mu and lambda alumina. *High Press. Res.* **1999**, *16*, 265–278. [CrossRef]
137. Bekheet, M.F.; Schwarz, M.R.; Lauterbach, S.; Kleebe, H.J.; Kroll, P.; Riedel, R.; Gurlo, A. Orthorhombic In_2O_3: A metastable polymorph of indium sesquioxide. *Angew. Chem. Int. Ed.* **2013**, *52*, 6531–6535. [CrossRef]
138. Karazhanov, S.Z.; Ravindran, P.; Vajeeston, P.; Ulyashin, A.; Finstad, T.G.; Fjellvåg, H. Phase stability, electronic structure, and optical properties of indium oxide polytypes. *Phys. Rev. B* **2007**, *76*, 075129. [CrossRef]
139. Shannon, R.D. New high pressure phases having the corundum structure. *Solid State Commun.* **1966**, *4*, 629–630. [CrossRef]
140. Prewitt, C.T.; Shannon, R.D.; Rogers, D.B.; Sleight, A.W. The C rare earth oxide-corundum transition and crystal chemistry of oxides having the corundum structure. *Inorg. Chem.* **1969**, *8*, 1985–1993. [CrossRef]
141. Atou, T.; Kusaba, K.; Fukuoka, K.; Kikuchi, M.; Syono, Y. Shock-induced phase transition of M_2O_3 (M = Sc, Y, Sm, Gd, and In)-type compounds. *J. Solid State Chem.* **1990**, *89*, 378–384. [CrossRef]
142. Epifani, M.; Siciliano, P.; Gurlo, A.; Barsan, N.; Weimar, U. Ambient Pressure Synthesis of Corundum-Type In_2O_3. *J. Am. Chem. Soc.* **2004**, *126*, 4078–4079. [CrossRef]
143. Yu, D.; Wang, D.; Qian, Y. Synthesis of metastable hexagonal In_2O_3 nanocrystals by a precursor-dehydration route under ambient pressure. *J. Solid State Chem.* **2004**, *177*, 1230–1234. [CrossRef]
144. Sorescu, M.; Diamandescu, L.; Tarabasanu-Mihaila, D.; Teodorescu, V.S. Nanocrystalline rhombohedral In_2O_3 synthesized by hydrothermal and postannealing pathways. *J. Mater. Sci.* **2004**, *39*, 675–677. [CrossRef]
145. Åhman, J.; Svensson, G.; Albertsson, J. A reinvestigation of β-gallium oxide. *Acta Crystallogr. Sect. C Cryst. Struct. Commun.* **1996**, *52*, 1336–1338. [CrossRef]
146. Geller, S. Crystal structure of β-Ga_2O_3. *J. Chem. Phys.* **1960**, *33*, 676–684. [CrossRef]
147. Remeika, J.P.; Marezio, M. Growth of α-Ga_2O_3 single crystals at 44 kbars. *Appl. Phys. Lett.* **1966**, *8*, 87–88. [CrossRef]
148. Tsuchiya, T.; Yusa, H.; Tsuchiya, J. Post-Rh_2O_3(II) transition and the high pressure-temperature phase diagram of gallia: A first-principles and x-ray diffraction study. *Phys. Rev. B* **2007**, *76*, 174108. [CrossRef]
149. Kishimura, H.; Matsumoto, H. Evaluation of the shock-induced phase transition in β-Ga_2O_3. *Jpn. J. Appl. Phys.* **2018**, *57*, 125503. [CrossRef]
150. Gurr, G.E.; Montgomery, P.W.; Knutson, C.D.; Gorres, B.T. The crystal structure of trigonal diboron trioxide. *Acta Crystallogr. Sect. B Struct. Crystallogr. Cryst. Chem.* **1970**, *26*, 906–915. [CrossRef]
151. Switzer, J.A. The n-Silicon/Thallium(III) Oxide Heterojunction Photoelectrochemical Solar Cell. *J. Electrochem. Soc.* **1986**, *133*, 722–728. [CrossRef]
152. Phillips, R.J.; Shane, M.J.; Switzer, J.A. Electrochemical and photoelectrochemical deposition of thallium(III) oxide thin films. *J. Mater. Res.* **1989**, *4*, 923–929. [CrossRef]

153. Van Leeuwen, R.A.; Hung, C.J.; Kammler, D.R.; Switzer, J.A. Optical and electronic transport properties of electrodeposited thallium(III) oxide films. *J. Phys. Chem.* **1995**, *99*, 15247–15252. [CrossRef]
154. Bhattacharya, R.N.; Yan, S.L.; Xing, Z.; Xie, Y.; Wu, J.Z.; Feldmann, M.; Chen, J.; Xiong, Q.; Ren, Z.F.; Blaugher, R.D. Superconducting Thallium Oxide and Mercury Oxide Films. *MRS Online Proc. Libr. Arch.* **2000**, *659*. [CrossRef]
155. Ma, C.; Rossman, G.R. Tistarite, Ti_2O_3, a new refractory mineral from the Allende meteorite. *Am. Mineral.* **2009**, *94*, 841–844. [CrossRef]
156. Xue, K.H.; Blaise, P.; Fonseca, L.R.C.; Nishi, Y. Prediction of semimetallic tetragonal Hf_2O_3 and Zr_2O_3 from first principles. *Phys. Rev. Lett.* **2013**, *110*, 065502. [CrossRef]
157. Ovsyannikov, S.V.; Trots, D.M.; Kurnosov, A.V.; Morgenroth, W.; Liermann, H.P.; Dubrovinsky, L. Anomalous compression and new high-pressure phases of vanadium sesquioxide, V_2O_3. *J. Phys. Condens. Matter* **2013**, *25*, 385401. [CrossRef]
158. Goodenough, J.B.; Hamnett, A.; Huber, G.; Hullinger, F.; Leiß, M.; Ramasesha, S.K.; Werheit, H. *Physics of Non-Tetrahedrally Bonded Binary Compounds III/Physik der Nicht-Tetraedrisch Gebundenen Binären Verbindungen III*; Madelung, O., Ed.; Springer: Berlin, Germany, 1984.
159. Pasternak, M.P.; Rozenberg, G.K.; Machavariani, G.Y.; Naaman, O.; Taylor, R.D.; Jeanloz, R. Breakdown of the mott-hubbard state in Fe_2O_3: A first-order insulator-metal transition with collapse of magnetism at 50 GPa. *Phys. Rev. Lett.* **1999**, *82*, 4663–4666. [CrossRef]
160. Frost, D.J.; Liebske, C.; Langenhorst, F.; McCammon, C.A.; Trønnes, R.G.; Rubie, D.C. Experimental evidence for the existence of iron-rich metal in the Earth's lower mantle. *Nature* **2004**, *428*, 409–412. [CrossRef]
161. Kupenko, I.; Aprilis, G.; Vasiukov, D.M.; McCammon, C.; Chariton, S.; Cerantola, V.; Kantor, I.; Chumakov, A.I.; Rüffer, R.; Dubrovinsky, L.; et al. Magnetism in cold subducting slabs at mantle transition zone depths. *Nature* **2019**, *570*, 102–106. [CrossRef]
162. Shokrollahi, H. A review of the magnetic properties, synthesis methods and applications of maghemite. *J. Magn. Magn. Mater.* **2017**, *426*, 74–81. [CrossRef]
163. Forestier, H.; Guiot-Guillain, G. Une nouvelle variété ferromagnétique de sesquioxyde de fer. *CR Acad. Sci. (Paris)* **1934**, *199*, 720–722.
164. Schrader, R.; Büttner, G. Eine neue Eisen(III)-oxidphase: ϵ-Fe_2O_3. *Z. Anorg. Allg. Chem.* **1963**, *320*, 220–234. [CrossRef]
165. Xu, H.; Lee, S.; Xu, H. Luogufengite: A new nano-mineral of Fe_2O_3 polymorph with giant coercive field. *Am. Mineral.* **2017**, *102*, 711–719. [CrossRef]
166. Dejoie, C.; Sciau, P.; Li, W.; Noé, L.; Mehta, A.; Chen, K.; Luo, H.; Kunz, M.; Tamura, N.; Liu, Z. Learning from the past: Rare ε-Fe_2O_3 in the ancient black-glazed Jian (Tenmoku) wares. *Sci. Rep.* **2015**, *4*, 4941. [CrossRef]
167. Tronc, E.; Chanéac, C.; Jolivet, J.P. Structural and Magnetic Characterization of ε-Fe_2O_3. *J. Solid State Chem.* **1998**, *139*, 93–104. [CrossRef]
168. Tuček, J.; Zbořil, R.; Namai, A.; Ohkoshi, S. ε-Fe_2O_3: An Advanced Nanomaterial Exhibiting Giant Coercive Field, Millimeter-Wave Ferromagnetic Resonance, and Magnetoelectric Coupling. *Chem. Mater.* **2010**, *22*, 6483–6505. [CrossRef]
169. Tuček, J.; Machala, L.; Ono, S.; Namai, A.; Yoshikiyo, M.; Imoto, K.; Tokoro, H.; Ohkoshi, S.; Zbořil, R. Zeta-Fe_2O_3—A new stable polymorph in iron(III) oxide family. *Sci. Rep.* **2015**, *5*, 15091. [CrossRef]
170. Rozenberg, G.K.; Dubrovinsky, L.S.; Pasternak, M.P.; Naaman, O.; Le Bihan, T.; Ahuja, R. High-pressure structural studies of hematite (Fe_2O_3). *Phys. Rev. B* **2002**, *65*, 064112. [CrossRef]
171. Badro, J.; Fiquet, G.; Struzhkin, V.V.; Somayazulu, M.; Mao, H.K.; Shen, G.; Le Bihan, T. Nature of the high-pressure transition in Fe_2O_3 hematite. *Phys. Rev. Lett.* **2002**, *89*, 205504. [CrossRef]
172. Ito, E.; Fukui, H.; Katsura, T.; Yamazaki, D.; Yoshino, T.; Aizawa, Y.; Kubo, A.; Yokoshi, S.; Kawabe, K.; Zhai, S.; et al. Determination of high-pressure phase equilibria of Fe_2O_3 using the Kawai-type apparatus equipped with sintered diamond anvils. *Am. Mineral.* **2009**, *94*, 205–209. [CrossRef]
173. Bykova, E.; Bykov, M.; Prakapenka, V.; Konôpková, Z.; Liermann, H.-P.; Dubrovinskaia, N.; Dubrovinsky, L. Novel high pressure monoclinic Fe_2O_3 polymorph revealed by single-crystal synchrotron X-ray diffraction studies. *High Press. Res.* **2013**, *33*, 534–545. [CrossRef]
174. Sanson, A.; Kantor, I.; Cerantola, V.; Irifune, T.; Carnera, A.; Pascarelli, S. Local structure and spin transition in Fe_2O_3 hematite at high pressure. *Phys. Rev. B* **2016**, *94*, 014112. [CrossRef]

175. Bykova, E.; Dubrovinsky, L.; Dubrovinskaia, N.; Bykov, M.; McCammon, C.; Ovsyannikov, S.V.; Liermann, H.P.; Kupenko, I.; Chumakov, A.I.; Rüffer, R.; et al. Structural complexity of simple Fe_2O_3 at high pressures and temperatures. *Nat. Commun.* **2016**, *7*, 10661. [CrossRef]
176. Greenberg, E.; Leonov, I.; Layek, S.; Konopkova, Z.; Pasternak, M.P.; Dubrovinsky, L.; Jeanloz, R.; Abrikosov, I.A.; Rozenberg, G.K. Pressure-Induced Site-Selective Mott Insulator-Metal Transition in Fe_2O_3. *Phys. Rev. X* **2018**, *8*, 31059. [CrossRef]
177. Liu, H.; Caldwell, A.; Benedetti, L.R.; Panero, W.; Jeanloz, R. Static compression of α-Fe_2O_3: Linear incompressibility of lattice parameters and high-pressure transformations. *Phys. Chem. Miner.* **2003**, *30*, 582–588. [CrossRef]
178. Olsen, J.S.; Cousins, C.S.G.; Gerward, L.; Jhans, H.; Sheldon, B.J. A study of the crystal structure of Fe_2O_3 in the pressure range up to 65 GPa using synchrotron radiation. *Phys. Scr.* **1991**, *43*, 327–330. [CrossRef]
179. Shim, S.H.; Bengtson, A.; Morgan, D.; Sturhahn, W.; Catalli, K.; Zhao, J.; Lerche, M.; Prakapenka, V. Electronic and magnetic structures of the postperovskite-type Fe_2O_3 and implications for planetary magnetic records and deep interiors. *Proc. Natl. Acad. Sci. USA* **2009**, *106*, 5508–5512. [CrossRef]
180. Syono, Y.; Ito, A.; Morimoto, S.; Suzuki, T.; Yagi, T.; Akimoto, S. Mössbauer study on the high pressure phase of Fe_2O_3. *Solid State Commun.* **1984**, *50*, 97–100. [CrossRef]
181. Nasu, S.; Kurimoto, K.; Nagatomo, S.; Endo, S.; Fujita, F.E. 57Fe Mössbauer study under high pressure; ε-Fe and Fe_2O_3. *Hyperfine Interact.* **1986**, *29*, 1583–1586. [CrossRef]
182. Jiang, J.Z.; Olsen, J.S.; Gerward, L.; Mørup, S. Enhanced bulk modulus and reduced transition pressure in γ-Fe_2O_3 nanocrystals. *Europhys. Lett.* **1998**, *44*, 620–626. [CrossRef]
183. Zhu, H.; Ma, Y.; Yang, H.; Ji, C.; Hou, D.; Guo, L. Pressure induced phase transition of nanocrystalline and bulk maghemite (γ-Fe_2O_3) to hematite (α-Fe_2O_3). *J. Phys. Chem. Solids* **2010**, *71*, 1183–1186. [CrossRef]
184. MacHala, L.; Tuček, J.; Zbořil, R. Polymorphous transformations of nanometric iron(III) oxide: A review. *Chem. Mater.* **2011**, *23*, 3255–3272. [CrossRef]
185. Hearne, G.; Pischedda, V. Pressure response of vacancy ordered maghemite (γ-Fe_2O_3) and high pressure transformed hematite (α-Fe_2O_3). *J. Solid State Chem.* **2012**, *187*, 134–142. [CrossRef]
186. Sans, J.A.; Monteseguro, V.; Garbarino, G.; Gich, M.; Cerantola, V.; Cuartero, V.; Monte, M.; Irifune, T.; Muñoz, A.; Popescu, C. Stability and nature of the volume collapse of ε-Fe_2O_3 under extreme conditions. *Nat. Commun.* **2018**, *9*, 4554. [CrossRef]
187. Grant, R.W.; Geller, S.; Cape, J.A.; Espinosa, G.P. Magnetic and crystallographic transitions in the α-Mn_2O_3-Fe_2O_3 system. *Phys. Rev.* **1968**, *175*, 686–695. [CrossRef]
188. Geller, S. Structure of α-Mn_2O_3, $(Mn_{0.983}Fe_{0.017})_2O_3$ and $(Mn_{0.37}Fe_{0.63})_2O_3$ and relation to magnetic ordering. *Acta Crystallogr. Sect. B Struct. Crystallogr. Cryst. Chem.* **1971**, *27*, 821–828. [CrossRef]
189. Yamanaka, T.; Nagai, T.; Okada, T.; Fukuda, T. Structure change of Mn_2O_3 under high pressure and pressure-induced transition. *Z. Kristallog.* **2005**, *220*, 938–945. [CrossRef]
190. Santillán, J.; Shim, S.H.; Shen, G.; Prakapenka, V.B. High-pressure phase transition in Mn_2O_3: Application for the crystal structure and preferred orientation of the $CaIrO_3$ type. *Geophys. Res. Lett.* **2006**, *33*, L15307. [CrossRef]
191. Shim, S.H.; LaBounty, D.; Duffy, T.S. Raman spectra of bixbyite, Mn_2O_3, up to 40 GPa. *Phys. Chem. Miner.* **2011**, *38*, 685–691. [CrossRef]
192. Mukherjee, G.D.; Vaidya, S.N.; Karunakaran, C. High Pressure and High Temperature Studies on Manganese Oxides. *Phase Transit.* **2002**, *75*, 557–566. [CrossRef]
193. Ovsyannikov, S.V.; Abakumov, A.M.; Tsirlin, A.A.; Schnelle, W.; Egoavil, R.; Verbeeck, J.; Van Tendeloo, G.; Glazyrin, K.V.; Hanfland, M.; Dubrovinsky, L. Perovskite-like Mn_2O_3: A path to new manganites. *Angew. Chem. Int. Ed.* **2013**, *52*, 1494–1498. [CrossRef]
194. Hong, F.; Yue, B.; Hirao, N.; Liu, Z.; Chen, B. Significant improvement in Mn_2O_3 transition metal oxide electrical conductivity via high pressure. *Sci. Rep.* **2017**, *7*, 44078. [CrossRef]
195. Ovsyannikov, S.V.; Karkin, A.E.; Morozova, N.V.; Shchennikov, V.V.; Bykova, E.; Abakumov, A.M.; Tsirlin, A.A.; Glazyrin, K.V.; Dubrovinsky, L. A hard oxide semiconductor with a direct and narrow bandgap and switchable p-n electrical conduction. *Adv. Mater.* **2014**, *26*, 8185–8191. [CrossRef]
196. Khalyavin, D.D.; Johnson, R.D.; Manuel, P.; Tsirlin, A.A.; Abakumov, A.M.; Kozlenko, D.P.; Sun, Y.; Dubrovinsky, L.; Ovsyannikov, S.V. Magneto-orbital texture in the perovskite modification of Mn_2O_3. *Phys. Rev. B* **2018**, *98*, 014426. [CrossRef]

197. McWhan, D.B.; Rice, T.M.; Remeika, J.P. Mott Transition in Cr-Doped V_2O_3. *Phys. Rev. Lett.* **1969**, *23*, 1384–1387. [CrossRef]
198. Lupi, S.; Baldassarre, L.; Mansart, B.; Perucchi, A.; Barinov, A.; Dudin, P.; Papalazarou, E.; Rodolakis, F.; Rueff, J.P.; Itié, J.P.; et al. A microscopic view on the Mott transition in chromium-doped V_2O_3. *Nat. Commun.* **2010**, *1*, 105. [CrossRef]
199. Weber, D.; Stork, A.; Nakhal, S.; Wessel, C.; Reimann, C.; Hermes, W.; Müller, A.; Ressler, T.; Pöttgen, R.; Bredow, T.; et al. Bixbyite-Type V_2O_3—A Metastable Polymorph of Vanadium Sesquioxide. *Inorg. Chem.* **2011**, *50*, 6762–6766. [CrossRef] [PubMed]
200. McWhan, D.B.; Remeika, J.P. Metal-Insulator Transition in $(V_{1-x}Cr_x)O_3$. *Phys. Rev. B* **1970**, *2*, 3734–3750. [CrossRef]
201. Jayaraman, A.; McWhan, D.B.; Remeika, J.P.; Dernier, P.D. Critical Behavior of the Mott Transition in Cr-Doped V_2O_3. *Phys. Rev. B* **1970**, *2*, 3751–3756. [CrossRef]
202. Carter, S.A.; Rosenbaum, T.F.; Lu, M.; Jaeger, H.M.; Metcalf, P.; Honig, J.M.; Spalek, J. Magnetic and transport studies of pure V_2O_3 under pressure. *Phys. Rev. B* **1994**, *49*, 7898–7903. [CrossRef] [PubMed]
203. Limelette, P.; Georges, A.; Jérome, D.; Wzietek, P.; Metcalf, P.; Honig, J.M. Universality and critical behavior at the Mott transition. *Science* **2003**, *302*, 89–92. [CrossRef]
204. Rodolakis, F.; Hansmann, P.; Rueff, J.-P.; Toschi, A.; Haverkort, M.W.; Sangiovanni, G.; Tanaka, A.; Saha-Dasgupta, T.; Andersen, O.K.; Held, K.; et al. Inequivalent Routes across the Mott Transition in V_2O_3 Explored by X-Ray Absorption. *Phys. Rev. Lett.* **2010**, *104*, 047401. [CrossRef]
205. Alyabyeva, N.; Sakai, J.; Bavencoffe, M.; Wolfman, J.; Limelette, P.; Funakubo, H.; Ruyter, A. Metal-insulator transition in V_2O_3 thin film caused by tip-induced strain. *Appl. Phys. Lett.* **2018**, *113*, 241603. [CrossRef]
206. Finger, L.W.; Hazen, R.M. Crystal structure and isothermal compression of Fe_2O_3, Cr_2O_3, and V_2O_3 to 50 kbars. *J. Appl. Phys.* **1980**, *51*, 5362–5367. [CrossRef]
207. Zhang, Q.; Wu, X.; Qin, S. Pressure-induced phase transition of V_2O_3. *Chin. Phys. Lett.* **2012**, *29*, 106101. [CrossRef]
208. Zhang, Q.; Wu, X.; Qin, S. A nine-fold coordinated vanadium by oxygen in V_2O_3 from first-principles calculations. *Eur. Phys. J. B* **2012**, *85*, 267. [CrossRef]
209. Aggarwal, P.S.; Goswami, A. An oxide of tervalent nickel. *J. Phys. Chem.* **1961**, *65*, 2105. [CrossRef]
210. Conell, R.S.; Corrigan, D.A.; Powell, B.R. The electrochromic properties of sputtered nickel oxide films. *Sol. Energy Mater. Sol. Cells* **1992**, *25*, 301–313. [CrossRef]
211. Jones, P.G.; Rumpel, H.; Schwarzmann, E.; Sheldrick, G.M. Gold (III) oxide. *Acta Cryst. B* **1979**, *35*, 1435–1437. [CrossRef]
212. Minomura, S.; Drickamer, H.G. Effect of Pressure on the Electrical Resistance of some Transition-Metal Oxides and Sulfides. *J. Appl. Phys.* **1963**, *34*, 3043–3048. [CrossRef]
213. Chenavas, J.; Joubert, J.C.; Marezio, M. Low-spin → high-spin state transition in high pressure cobalt sesquioxide. *Solid State Commun.* **1971**, *9*, 1057–1060. [CrossRef]
214. Rekhi, S.; Dubrovinsky, L.S.; Ahuja, R.; Saxena, S.K.; Johansson, B. Experimental and theoretical investigations on eskolaite (Cr_2O_3) at high pressures. *J. Alloy. Compd.* **2000**, *302*, 16–20. [CrossRef]
215. Kota, Y.; Yoshimori, Y.; Imamura, H.; Kimura, T. Enhancement of magnetoelectric operating temperature in compressed Cr_2O_3 under hydrostatic pressure. *Appl. Phys. Lett.* **2017**, *110*, 042902. [CrossRef]
216. Kantor, A.; Kantor, I.; Merlini, M.; Glazyrin, K.; Prescher, C.; Hanfland, M.; Dubrovinsky, L. High-pressure structural studies of eskolaite by means of single-crystal X-ray diffraction. *Am. Mineral.* **2012**, *97*, 1764–1770. [CrossRef]
217. Shim, S.H.; Duffy, T.S.; Jeanloz, R.; Yoo, C.S.; Iota, V. Raman spectroscopy and x-ray diffraction of phase transitions in Cr_2O_3 to 61 GPa. *Phys. Rev. B* **2004**, *69*, 144107. [CrossRef]
218. Dobin, A.Y.; Duan, W.; Wentzcovitch, R.M. Magnetostructural effects and phase transition in Cr_2O_3 under pressure. *Phys. Rev. B* **2000**, *62*, 11997–12000. [CrossRef]
219. Golosova, N.O.; Kozlenko, D.P.; Kichanov, S.E.; Lukin, E.V.; Liermann, H.-P.; Glazyrin, K.V.; Savenko, B.N. Structural and magnetic properties of Cr_2O_3 at high pressure. *J. Alloy. Compd.* **2017**, *722*, 593–598. [CrossRef]
220. Nishio-Hamane, D.; Katagiri, M.; Niwa, K.; Sano-Furukawa, A.; Okada, T.; Yagi, T. A new high-pressure polymorph of Ti_2O_3: Implication for high-pressure phase transition in sesquioxides. *High Press. Res.* **2009**, *29*, 379–388. [CrossRef]

221. Umemoto, K.; Wentzcovitch, R.M. Prediction of an U_2S_3-type polymorph of Al_2O_3 at 3.7 Mbar. *Proc. Natl. Acad. Sci. USA* **2008**, *105*, 6526–6530. [CrossRef] [PubMed]
222. Ovsyannikov, S.V.; Wu, X.; Shchennikov, V.V.; Karkin, A.E.; Dubrovinskaia, N.; Garbarino, G.; Dubrovinsky, L. Structural stability of a golden semiconducting orthorhombic polymorph of Ti_2O_3 under high pressures and high temperatures. *J. Phys. Condens. Matter* **2010**, *22*, 375402. [CrossRef] [PubMed]
223. Ovsyannikov, S.V.; Wu, X.; Karkin, A.E.; Shchennikov, V.V.; Manthilake, G.M. Pressure-temperature phase diagram of Ti_2O_3 and physical properties in the golden Th_2S_3-type phase. *Phys. Rev. B* **2012**, *86*, 024106. [CrossRef]
224. Ovsyannikov, S.V.; Wu, X.; Garbarino, G.; Núñez-Regueiro, M.; Shchennikov, V.V.; Khmeleva, J.A.; Karkin, A.E.; Dubrovinskaia, N.; Dubrovinsky, L. High-pressure behavior of structural, optical, and electronic transport properties of the golden Th_2S_3-type Ti_2O_3. *Phys. Rev. B* **2013**, *88*, 184106. [CrossRef]
225. Biesterbos, J.W.M.; Hornstra, J. The Crystal Structure of the high-temperature low-pressure form of Rh_2O_3. *J. Less Common Met.* **1973**, *30*, 121–125. [CrossRef]
226. Shannon, R.D.; Prewitt, C.T. Synthesis and structure of a new high-pressure form of Rh_2O_3. *J. Solid State Chem.* **1970**, *2*, 134–136. [CrossRef]
227. Zhuo, S.; Sohlberg, K. Origin of stability of the high-temperature, low-pressure Rh_2O_3 III form of rhodium sesquioxide. *J. Solid State Chem.* **2006**, *179*, 2126–2132. [CrossRef]
228. Becker, N.; Reimann, C.; Weber, D.; Lüdtke, T.; Lerch, M.; Bredow, T.; Dronskowski, R. A density-functional theory approach to the existence and stability of molybdenum and tungsten sesquioxide polymorphs. *Z. Kristallogr.* **2017**, *232*, 69–75. [CrossRef]
229. Zhang, J.; Oganov, A.R.; Li, X.; Xue, K.H.; Wang, Z.; Dong, H. Pressure-induced novel compounds in the Hf-O system from first-principles calculations. *Phys. Rev. B* **2015**, *92*, 184104. [CrossRef]
230. Ai, Z.; Huang, Y.; Lee, S.; Zhang, L. Monoclinic α-Bi_2O_3 photocatalyst for efficient removal of gaseous NO and HCHO under visible light irradiation. *J. Alloy. Compd.* **2011**, *509*, 2044–2049. [CrossRef]
231. Zheng, F.L.; Li, G.R.; Ou, Y.N.; Wang, Z.L.; Su, C.Y.; Tong, Y.X. Synthesis of hierarchical rippled Bi_2O_3 nanobelts for supercapacitor applications. *Chem. Commun.* **2010**, *46*, 5021–5023. [CrossRef] [PubMed]
232. Hu, M.; Jiang, Y.; Sun, W.; Wang, H.; Jin, C.; Yan, M. Reversible Conversion-Alloying of Sb_2O_3 as a High-Capacity, High Rate, and Durable Anode for Sodium Ion Batteries. *ACS Appl. Mater. Interfaces* **2014**, *6*, 19449–19455. [CrossRef] [PubMed]
233. Datta, A.; Giri, A.K.; Chakravorty, D. AC conductivity of Sb_2O_3-P_2O_5 glasses. *Phys. Rev. B* **1993**, *47*, 16242. [CrossRef]
234. Shen, Z.-X.; Chen, G.-Q.; Ni, J.-H.; Li, X.-S.; Xiong, S.-M.; Qiu, Q.-Y.; Zhu, J.; Tang, W.; Sun, G.-L.; Yang, K.-Q.; et al. Use of Arsenic Trioxide (As_2O_3) in the Treatment of Acute Promyelocytic Leukemia (APL): II. Clinical Efficacy and Pharmacokineticsin Relapsed Patients. *Blood* **1997**, *89*, 3354–3360. [CrossRef]
235. Shen, Z.-X.; Shi, Z.-Z.; Fang, J.; Gu, B.-W.; Li, J.-M.; Zhu, Y.-M.; Shi, J.-Y.; Zheng, P.-Z.; Yan, H.; Liu, Y.F.; et al. All-trans retinoic acid/As_2O_3 combination yields a high quality remission and survival in newly diagnosed acute promyelocytic leukemia. *Proc. Natl. Acad. Sci. USA* **2004**, *101*, 5328–5335. [CrossRef]
236. Matsumoto, A.; Koyama, Y.; Togo, A.; Choi, M.; Tanaka, I. Electronic structures of dynamically stable As_2O_3, Sb_2O_3, and Bi_2O_3 crystal polymorphs. *Phys. Rev. B* **2011**, *83*, 214110. [CrossRef]
237. Matsumoto, A.; Koyama, Y.; Tanaka, I. Structures and energetics of Bi_2O_3 polymorphs in a defective fluorite family derived by systematic first-principles lattice dynamics calculations. *Phys. Rev. B* **2010**, *81*, 094117. [CrossRef]
238. Zhao, Z.; Zeng, Q.; Zhang, H.; Wang, S.; Hirai, S.; Zeng, Z.; Mao, W.L. Structural transition and amorphization in compressed α-Sb_2O_3. *Phys. Rev. B* **2015**, *91*, 184112. [CrossRef]
239. Sans, J.A.; Manjón, F.J.; Popescu, C.; Cuenca-Gotor, V.P.; Gomis, O.; Muñoz, A.; Rodríguez-Hernández, P.; Contreras-García, J.; Pellicer-Porres, J.; Pereira, A.L.J.; et al. Ordered helium trapping and bonding in compressed arsenolite: Synthesis of As_4O_6·2He. *Phys. Rev. B* **2016**, *93*, 054102. [CrossRef]
240. Cuenca-Gotor, V.P.; Gomis, O.; Sans, J.A.; Manjon, F.J.; Rodrıguez-Hernandez, P.; Muñoz, A. Vibrational and elastic properties of As_4O_6 and As_4O_6·2He at high pressures: Study of dynamical and mechanical stability. *J. Appl. Phys.* **2016**, *120*, 155901. [CrossRef]
241. Guńka, P.A.; Dziubek, K.F.; Gładysiak, A.; Dranka, M.; Piechota, J.; Hanfland, M.; Katrusiak, A.; Zachara, J. Compressed Arsenolite As4O6 and Its Helium Clathrate As_4O_6·2He. *Cryst. Growth Des.* **2015**, *15*, 3740–3745. [CrossRef]

242. Pereira, A.L.J.; Gracia, L.; Santamaría-Pérez, D.; Vilaplana, R.; Manjón, F.J.; Errandonea, D.; Nalin, M.; Beltrán, A. Structural and vibrational study of cubic Sb_2O_3 under high pressure. *Phys. Rev. B* **2012**, *85*, 174108. [CrossRef]
243. Pereira, A.L.J.; Sans, J.A.; Vilaplana, R.; Gomis, O.; Manjón, F.J.; Rodríguez-Hernández, P.; Muñoz, A.; Popescu, C.; Beltrán, A. Isostructural Second-Order Phase Transition of β-Bi_2O_3 at High Pressures: An Experimental and Theoretical Study. *J. Phys. Chem. C* **2014**, *118*, 23189–23201. [CrossRef]
244. Orosel, D.; Dinnebier, R.E.; Blatov, V.A.; Jansen, M. Structure of a new high-pressure–high-temperature modification of antimony(III) oxide, γ-Sb_2O_3, from high-resolution synchrotron powder diffraction data. *Acta Cryst. B* **2012**, *68*, 1–7. [CrossRef]
245. Cornei, N.; Tancret, N.; Abraham, F.; Mentré, O. New ε-Bi_2O_3 Metastable Polymorph. *Inorg. Chem.* **2006**, *45*, 4886–4888. [CrossRef]
246. Zou, Y.; Zhang, W.; Li, X.; Ma, M.; Li, X.; Wang, C.-H.; He, B.; Wang, S.; Chen, Z.; Zhao, Y.; et al. Pressure-induced anomalies and structural instability in compressed β-Sb_2O_3. *Phys. Chem. Chem. Phys.* **2018**, *20*, 11430–11436. [CrossRef]
247. Geng, A.-H.; Cao, L.-H.; Ma, Y.-M.; Cui, Q.-L.; Wan, C.-M. Experimental Observation of Phase Transition in Sb_2O_3 under High Pressure. *Chin. Phys. Lett.* **2016**, *33*, 097401. [CrossRef]
248. Harwig, H.A. On the Structure of Bismuthsesquioxide: The α, β, γ, and δ-Phase. *Z. Anorg. Allg. Chem.* **1978**, *444*, 151–166. [CrossRef]
249. Pereira, A.L.J.; Errandonea, D.; Beltrán, A.; Gracia, L.; Gomis, O.; Sans, J.A.; García-Domene, B.; Miquel-Veyrat, A.; Manjón, F.J.; Muñoz, A.; et al. Structural study of α-Bi_2O_3 under pressure. *J. Phys. Condens. Matter* **2013**, *25*, 475402. [CrossRef] [PubMed]
250. Gavriliuk, A.G.; Struzhkin, V.; Lyubutin, S.; Eremets, I.; Trojan, A.; Artemov, V. Equation of state and high-pressure irreversible amorphization in $Y_3Fe_5O_{12}$. *JETP Lett.* **2006**, *83*, 37–41. [CrossRef]
251. Locherer, T.; Dasari, L.; Prasad, V.K.; Dinnebier, R.; Wedig, U.; Jansen, M. High-pressure structural evolution of HP-Bi_2O_3. *Phys. Rev. B* **2011**, *83*, 214102. [CrossRef]
252. Ghedia, S.; Locherer, T.; Dinnebier, R.; Prasad, D.L.V.K.; Wedig, U.; Jansen, M.; Senyshyn, A. High-pressure and high-temperature multianvil synthesis of metastable polymorphs of Bi_2O_3: Crystal structure and electronic properties. *Phys. Rev. B* **2010**, *82*, 024106. [CrossRef]
253. Frueh, A.J., Jr. The crystal structure of claudetite (monoclinic As_2O_3). *Am. Miner.* **1951**, *36*, 833–850.
254. Pertlik, F. Die Kristallstruktur der monoklinen Form von As_2O_3 (Claudetit II). *Mon. Chem.* **1975**, *106*, 755–762. [CrossRef]
255. Soignard, E.; Amin, S.A.; Mei, Q.; Benmore, C.J.; Yarger, J.L. High-pressure behavior of As_2O_3: Amorphous-amorphous and crystalline-amorphous transitions. *Phys. Rev. B* **2008**, *77*, 144113. [CrossRef]
256. Guńka, P.A.; Dranka, M.; Piechota, J.; Żukowska, G.Z.; Zalewska, A.; Zachara, J. As_2O_3 Polymorphs: Theoretical Insight into Their Stability and Ammonia Templated Claudetite II Crystallization. *Cryst. Growth Des.* **2012**, *12*, 5663–5670. [CrossRef]
257. Guńka, P.A.; Dranka, M.; Hanfland, M.; Dziubek, K.F.; Katrusiak, A.; Zachara, J. Cascade of High-Pressure Transitions of Claudetite II and the First Polar Phase of Arsenic(III) Oxide. *Cryst. Growth Des.* **2015**, *15*, 3950–3954. [CrossRef]
258. Jansen, M.; Moebs, M. Structural Investigations on Solid Tetraphosphorus Hexaoxide. *Inorg. Chem.* **1984**, *23*, 4486–4488. [CrossRef]
259. Clark, G.L.; Schieltz, N.C.; Quirke, T.T. A New Study of the Preparation and Properties of the Higher Oxides of Lead. *J. Am. Chem. Soc.* **1937**, *59*, 2305–2308. [CrossRef]
260. Bouvaist, J.; Weigel, D. Sesquioxyde de plomb, Pb_2O_3. I. Determination de la structure. *Acta Cryst. A* **1970**, *26*, 501–510. [CrossRef]
261. Seko, A.; Togo, A.; Oba, F.; Tanaka, I. Structure and Stability of a Homologous Series of Tin Oxides. *Phys. Rev. Lett.* **2008**, *100*, 045702. [CrossRef] [PubMed]
262. Zhao, J.-H.; Tan, R.-Q.; Yang, Y.; Xu, W.; Li, J.; Shen, W.-F.; Wu, G.-Q.; Yang, X.-F.; Song, W.-J. Synthesis mechanism of heterovalent Sn_2O_3 nanosheets in oxidation annealing process. *Chin. Phys. B* **2015**, *24*, 070505. [CrossRef]
263. Kuang, X.L.; Liu, T.M.; Zeng, W.; Peng, X.H.; Wang, Z.C. Hydrothermal synthesis and characterization of novel Sn_2O_3 hierarchical nanostructures. *Mat. Lett.* **2016**, *165*, 235–238. [CrossRef]
264. Imre, A.R. On the existence of negative pressure states. *Phys. Stat. Sol. (b)* **2007**, *244*, 893–899. [CrossRef]

265. McMillan, P.F. New materials from high-pressure experiments. *Nat. Mater.* **2002**, *1*, 19–25. [CrossRef]
266. Manjón, F.J.; Errandonea, D.; López-Solano, J.; Rodríguez-Hernández, P.; Muñoz, A. Negative pressures in $CaWO_4$ nanocrystals. *J. Appl. Phys.* **2009**, *105*, 094321. [CrossRef]
267. Matsui, T.; Yagasaki, T.; Matsumoto, M.; Tanaka, H. Phase diagram of ice polymorphs under negative pressure considering the limits of mechanical stability. *J. Phys. Chem.* **2019**, *150*, 041102. [CrossRef]